Title:

Over-expression of thyroid hormone receptor β2 in zebrafish changes the distribution of cone spectral signals.

Abbreviated Title:

Spectral changes with trβ2 overexpression

Author names and affiliations:

Ralph F. Nelson[1], Annika Balraj[1,2], Tara Suresh[1,3], Leah J. Elias[1,4], Takeshi Yoshimatsu[5,6] and Sara S. Patterson[1,7]

[1]National Institute of Neurological Disorders and Stroke, National Institutes of Health, Rockville, Maryland 20892

[2]Department of Anatomy and Biology, George Washington University, Washington DC, 20052

[3]Washington University School of Medicine, St. Louis, MO, 63110

[4]Neuroscience, Johns Hopkins Medical School, Baltimore, MD 21205

[5]Department of Biological Structure, University of Washington, Seattle, Washington 98195

[6]School of Life Sciences, University of Sussex, Brighton, UK

[7]Center for Visual Science, University of Rochester, New York, 14627

Submitting and corresponding author email address:

Ralph F. Nelson, nelsonr@ninds.nih.gov

Number of pages:

35

Number of figures:

13

Number of tables:

0

Number of words for Abstract:

223 of 250

Number of words for Introduction:

629 of 650

Number of words for Discussion:

1455 of 1500

Conflict of interest statement:

No conflicts of interest

Acknowledgements:

This work was supported by The Intramural Program of the National Institutes of Neurological Disorders and Stroke, National Institutes of Health, Bethesda, Maryland and by National Institutes of Health Grant EY14356 (to Rachel O. L. Wong). Current affiliations: AB, Department of Anatomy and Biology, George Washington University, District of Columbia; TS, Washington University School of Medicine, St Louis, Missouri; LE, Neuroscience, The Johns Hopkins University School of Medicine, Baltimore; TY, School of Life Sciences, University of Sussex, Brighton; SSP, Center for Visual Science, University of Rochester, New York.

Abstract

Thyroid hormone receptor β2 (trβ2), a splice variant of thyroxin receptor β, is a transcription factor/nuclear receptor selectively expressed in vertebrate long-wavelength-sensitive (LWS/red) retinal cones and essential for LWS cone development. Using two gain-of-function zebrafish transgenics, we examine the physiological and morphological impact of excess trβ2 in zebrafish cone specification. The *crx:mYFP-2A-trβ2* transgenic expresses trβ2 early, in retinal progenitors, while *gnat2:mYFP-2A-trβ2;mpv17*$^{-/-}$ expresses trβ2 later, in differentiated cone cells. Here electroretinographic signals are isolated from cones by synaptic blockade and the cone spectral composition analyzed. In 5-day *crx:mYFP-2A-trβ2* embryos, UV- and blue-cone signals are attenuated while LWS2 (larval red-cone opsin) amplitudes increase. 5-day *gnat2:mYFP-2A-trβ2;mpv17*$^{-/-}$ spectra are indistinguishable from controls but LWS2 signals surpass controls during later embryonic and juvenile stages. By adulthood, both transgenics become entirely, or almost entirely, red cone dichromats, with LWS1 (adult red-cone opsin) amplitudes becoming super-normal, exceeding adult LWS2 signals, which are unchanged. Adult control LWS1 and LWS2 signal amplitudes are about equal. There are mixed opsin cones in both transgenic larvae. In *gnat2:mYFP-2A-trβ2;mpv17*$^{-/-}$, mixed UV- red- opsin immunoreactive cones, a reporter for the UV opsin gene is suppressed, suggesting a UV-to-red cone transformation process. Larval cones with gain-of-function transgenes are morphologically distinct from red, blue or UV cones, with wider inner segments and shorter axons than red cones, suggesting both cone spectral specification and shape are influenced by trβ2.

Significance Statement

Specification of neuronal type and function is critical to nervous system development. Expression of the *trβ2* gene in retinal neuronal progenitors or differentiated retinal cone cells appears to drive cells not destined to be LWS (red) cones towards that fate. The time of trβ2 insertion during development determines the speed of the transition.

Introduction

Thyroid hormone receptor β2 (trβ2), a splice variant of the *thrb* gene, is selectively expressed in vertebrate retinal cones (Ng et al., 2001). When deleted, cones expressing opsins in the long-wavelength-sensitive (LWS) subfamily of the opsin molecular phylogenetic tree (Terakita, 2005) fail to be produced. This includes the MWS cones of mouse (Ng et al., 2001), human MWS and LWS cone function (Weiss et al., 2012), and both LWS1 and LWS2 red-cone signals of zebrafish (Deveau et al., 2020). The LWS cone subfamily senses the longest wavelengths a species detects, with opsin spectral peaks ranging from 511 nm in mouse (Jacobs et al., 1991) to 625 nm in goldfish (Marks, 1965). Although trβ2 is like a binary ON/OFF switch for LWS-cone development, the analogue expression level has import. Dilution of trβ2 in adult zebrafish *trβ2* $^{+/-}$ animals makes red cones less dense and depresses long-wavelength spectral sensitivity (Deveau et al., 2020). In embryonic and juvenile zebrafish binding of thyroid hormone (TH) may increase trβ2 potency. Unbound trβ2 suffices for red-cone development (Mackin et al., 2019). TH switches individual LWS2 red cones to LWS1 types. Reduction of TH through athyroidism switches LWS1 red cones to LWS2 (Mackin et al., 2019). TH depresses the expression of both SWS1- (UV-opsin) and SWS2- (blue-opsin) message (Mackin et al., 2019). TH and trβ2 are further involved in the preferential expression of several of the tandem quadruplicate RH2 cone opsins in zebrafish (Mackin et al., 2019). It appears likely that TH and trβ2 are upstream regulators in the specification of all cone types, though only trβ2 is essential for the red cone neuronal specification.

We examine the spectral, developmental, and morphological impacts of trβ2 overexpression in two gain-of-function zebrafish. In the first *crx:mYFP-2A-trβ2* (*crx:trβ2*) (Suzuki et al., 2013), trβ2 is promoted by the cone-rod homeobox gene (*crx*), active by day 2 in larval development, at the embryonic neural progenitor stage (Shen and Raymond, 2004; Suzuki et al., 2013). In the second *gnat2:mYFP-2A-trβ2;mpv17*$^{-/-}$ (*gnat2:trβ2*) (Suzuki et al., 2013), trβ2 is promoted by *gnat2*, the cone transducin α promoter (Brockerhoff et al., 2003; Kennedy et al., 2007). This introduces trβ2 later in development, and only into differentiated retinal cones. In previous studies, during morpholino knockdown of native trβ2, larval *crx:trβ2* retinas overproduced red-opsin immunoreactive cones and underproduced RH2- (green), SWS2- (blue) and SWS1- (UV) opsin immunoreactive cones. In larval *gnat2:trβ2* retinas, there was little change in the densities of cones immunoreactive for LWS-, Rh2-, SWS2- or SWS1- opsins, but 60% of RH2- and UV- immunoreactive cones expressed LWS opsins, becoming mixed-opsin types (Suzuki et al., 2013). Zebrafish transgenic mixed-opsin cones were thought to model rodent cones that natively express both UV and MWS opsins (Applebury et al., 2000).

The seminal morphological studies of these gain-of-function transgenics (Suzuki et al., 2013) beg further investigation to clarify the scope of trβ2 action. For example, does a single transgene induce physiologically and morphologically normal LWS cones by additionally promoting the full complement of genes required, and does trβ2 concentration influence the choice of functional LWS1 or LWS2 electrophysiology? Analysis of *gnat2:mYFP-2A-trβ2* spectral properties might reveal whether electrophysiological integration occurs when a foreign transcription factor and foreign opsin are introduced into an already differentiated cone of another sort, whether such non-native opsins would function at all in a foreign phototransduction cascade, and whether mixed opsin expression is a stable endpoint in cone development or a transitional state. Finally, the long-term developmental consequences of altered trβ2 expression for adult retinas are unknown, and might result in either retinal disease, or a spectrally unique visual system. We infer the activities of cone types in gain-of-function retinas through analysis of the spectral properties of the Aspartate-isolated cone component of the zebrafish ERG and examine the alteration in the developmental progression of signals from these cone types.

Materials and Methods

Zebrafish husbandry and experimental design

The gain-of-function and reporter-line zebrafish (*Danio rerio*) transgenics *crx:mYFP-2A-trβ2*, *gnat2:mYFP-2A-trβ2;mpv17*$^{-/-}$, *trβ2:tdTomato*;*sws1:GFP, sws1:nfsBmCherry* and *sws2:GFP* (Takechi et al., 2003; Takechi et al., 2008; Suzuki et al., 2013) were generously supplied by the Rachel Wong lab (University of Washington). In gain-of-function studies, fish were obtained by outcrosses such that control, and transgenic heterozygotes, were siblings (Fig. 1A), studied in random order on the same experimental days throughout larval development. The transgenic *gnat:mYFP-2A-trβ2* was maintained on an *mpv17*$^{-/-}$ (*roy orbison*) background (D'Agati et al., 2017) (Fig. 1C). There are several studied mutations of *mpv17* all with loss of irridophores (Bian et al., 2021). Here we use the naturally occurring 19-base-pair intronic deletion of the *roy orbison* mutant (D'Agati et al., 2017). The lack of reflective iridophores in the iris of this mutant facilitated phenotyping of pupil fluorescence. Pineal fluorescence was also a *gnat:mYFP-2A-trβ2;mpv17* characteristic.

Larval physiology was collected on days 5, 6, 7 and 12 post fertilization (dpf). For 5-7 dpf, larvae were incubated at 28° C in 3.5-inch Petri dishes atop a heating pad. Larval medium contained 60 mg/liter sea salt, 75 µl/liter 1.5% methylene blue (Sigma-Aldrich Cat. No. 03978). 5-7 dpf larvae were not fed. The methylene blue was omitted for live confocal microscopy because of its fluorescence. 8-12-day larvae were kept in system nursery tanks (520-650 µΩ water, 28° C, pH 7.5-7.7) and fed both Larval AP100 (Pentair Aquatic Eco-Systems) and live rotifers (*Brachionus plicatilis*; Reed Mariculture).

Some larvae were raised to adulthood (8-18 months) both for physiological studies and for retention as breeders. These were housed in stand-alone, recirculating, Aquatic Habitats benchtop systems (Pentair Aquatic Eco-Systems, Apopka, Florida). Adults were fed pulverized TetraMin flakes (Tetra GMBH) and live rotifers. The protocols for breeding and experimentation were approved by the National Institute of Neurological Disorders and Stroke / National Institute on Deafness and Other Communication Disorders / National Center for Complementary and Integrative Health IACUC (ASPs 1307, 1227).

Preparation and perfusion of Isolated eyes for physiology

Larvae were captured with disposable pipettes and placed on a glass lantern slide. After removing excess water, larvae were adsorbed onto a chip of black nitrocellulose filter paper (Millipore, 0.45 mm pore, Cat. No. HABP02500, MilliporeSigma), and decapitated (without anesthetic) using a long (37 mm) insect pin (Carolina Biological Supply). Using a binocular microscope (MZ12-5; Leica Microsystems), a longitudinal, dorsal-ventral cut through the head proptosed and isolated larval eyes, which were positioned facing up, taking care not to touch the eye directly. In the recording chamber, larval eyes as mounted on the nitrocellulose chip were perfused at 0.1 ml/min with Minimal Essential Medium (MEM; Thermo Fisher Scientific Cat. No. 11090-099, equilibrated with 95% O_2 and 5% CO_2) using a syringe pump (New Era 500L; Braintree Scientific) and a 28-guage microfil syringe needle as applicator (MF28G67; World Precision Instruments). The chamber was an inverted lid for a 35-mm culture dish (ThermoFisher Scientific), with a disk of 41-µm-mesh nylon filter (Millipore) covering the bottom to wick away perfusate. The perfusion applicator was positioned on the nylon mesh. 20 mM L-Aspartate (Sigma-Aldrich), added to the MEM perfusate, blocked post-synaptic, glutamatergic, photoreceptor mechanisms leaving only photoreceptor signals (Sillman et al., 1969). Patch electrodes (3 µm tip) were inserted trans-corneally (Fig. 1b) to record the isolated cone ERG signals (cone PIII) (Wong et al., 2004).

Adult eyecups were prepared from eyes removed from fish decapitated with a fresh, single-edged razor. Corneas and lenses were removed from the isolated eyes mounted upright on a 5-10 mm square of black nitrocellulose paper, and the preparation was placed in a recording chamber (as above). The perfusion

applicator was placed directly above the retina oxygenating the vitreal surface with MEM containing 10 mM L-Aspartate at 0.3 ml/min. Microelectrodes broken to 300 µm tip diameter placed in the eyecup recorded cone-PIII ERG signals (Nelson and Singla, 2009).

Live imaging of larval retinas

Transgenic larvae were raised at 28°C in 300 µM Phenylthiourea (PTU, Sigma-Aldrich) to prevent melanin formation in the pigment epithelium and allow imaging of the retina. At 6 dpf, each larva was mounted individually in 1.5% agarose (Sigma-Aldrich type VII-A) on an 8-chamber slide with the right eye against the cover-glass floor of the chamber. Eyes were imaged in z-stacks on Zeiss 880 confocal microscope at either 25x or 40x magnification at 1024-×-1024-pixel resolution. Cone morphometrics were measured in Fiji (ImageJ) on the optical slice that offered the longest stretch of resolved cones for 5 or 6 fish in each transgenic line. These measurements were analyzed for differences using a one-way ANOVA and Tukey's post-hoc test. Fluorescent reporters identified the morphology of wild type (WT) red and UV cones in eyes from *trβ2:tdTomato;sws1:GFP* (Fig. 1D) and of transgenic *gnat:mYFP-2A-trβ2* cones (Fig. 1F). In *crx:mYFP-2A-trβ2*, reporter fluorescence appeared in both cones and bipolar cells (Fig. 1E) as previously seen in antibody staining for Crx in zebrafish (Shen and Raymond, 2004).

Immunohistochemistry

Larvae were euthanized by icing, and then fixed in 4% paraformaldehyde (PFA) in 0.1M phosphate-buffered saline (PBS), pH 7.4, for 25 min at room temperature. Retinas were dissected in PBS using a pair of 30-gauge syringe needles, blocked in a solution containing 5% normal donkey serum and phosphate-buffered Triton X-100 0.5% (PBT) for 1–24 h and then incubated with primary antibodies. Triton X-100 was added to enhance antibody penetration. Primary antibodies included anti-ultraviolet opsin (rabbit, 1:500, kindly provided by David Hyde), anti-ultraviolet opsin (rabbit, 1:5,000, kindly provided by Jeremy Nathans), anti-blue opsin (rabbit, 1:5,000, kindly provided by Jeremy Nathans) and anti-rod opsin (1D4, mouse, 1:100, Santa Cruz: cs-57432), the later raised against bovine rhodopsin but recognizing red-cone outer segments in zebrafish (Yin et al., 2012). These were diluted into the blocking solution. After incubating for 4 days at 4 °C, samples were washed three times, 15 min each, in PBT and incubated for 1 day with secondary antibodies (DyLight 649 donkey anti-mouse and Alexa 594 donkey anti-rabbit, 1:500 each, Jackson ImmunoReseach) diluted in blocking solution. After three, 15 min washes (PBT), immunostained retinas were mounted in 0.5% agarose and cover slipped with Vectashield mounting medium (Vector). Confocal image stacks were acquired on a Leica SP8 microscope using a 1.0 NA 63×oil-immersion objective lens. Images were typically acquired with an XY resolution of 0.077 µm per pixel and 0.25 µm-thick Z slices (Yoshimatsu et al., 2014).

Spectral stimulus protocol

Larval eyes and adult eyecups were stimulated with nine wavelengths ranging from 330 nm to 650 nm (20-nm half-width interference filters, 40-nm increments, Chroma Technology). Seven intensities were presented at each wavelength (UV compliant neutral density filters, 0.5 log unit increments covering 3 log units, Andover Corporation). A calibrated photodiode (Newport Corporation) was used to determine stimulus irradiance in quantal units. This was placed in the plane of the cornea for larval eyes or the plane of the retina for adult eyecups. All spectral model calculations are based on absolute, wavelength-specific photodiode calibrations of quanta delivered to the eye. The light source is a 150W OFR Xenon arc with two optical channels gated by Uniblitz shutters (Vincent Associates). The stimulus channel passed through three Sutter filter wheels, through a UV-visible compliant liquid light guide (Sutter Instruments), through the epifluorescence port of the BX51WI upright microscope (Olympus –Life Science Solutions), and through either a 10 × UPlanFLN/0.3 microscope objective (larvae) or a 4 × UPlanSApo/0.16 objective (adults). The second optical channel passed through hand-inserted filters and an infrared

compliant liquid light guide (Newport Corporation) providing infrared (IR) side illumination for visualization and 'neutral' backgrounds, or through a 627 nm interference filter for red adapting backgrounds.

The spectral protocol was a fixed sequence of 280, 300 msec, monochromatic light flashes of different irradiances and wavelengths delivered by computer using in house software. Among these stimuli were 64 unique irradiance-wavelength combinations and 6 replicates delivered 10 minutes apart as an amplitude-stability check during the 20-min protocol. The 280 stimuli created a set of 70, 4X-averaged, electroretinogram (ERG) responses, the 'spectral dataset'. The interval between stimuli varied between 2.5 and 6 s, with the longer intervals separating the brighter stimuli. The maximal irradiances in log(quanta$\cdot\mu m^{-2}\cdot s^{-1}$) in the stimulus protocol were 7.2 (650 nm), 6.3 (610 nm), 6.4 (570 nm), 6.3 (530 nm), 6.4 (490 nm), 6.1 (450 nm), 5.7 (410 nm), 5.7 (370 nm), and 5.2 (330 nm).

To record a spectral dataset, the stimulating objective was positioned over the eye with a translation stage (MT-800; Sutter Instrument). Microelectrodes were inserted into eyes or eyecups with a micro-positioner (Sutter Instrument, MPC-385). ERG signals from the microelectrode were amplified by 10,000 (World Precision Instruments, DAM80, 0.1 Hz-1k Hz bandpass), and digitized (2000 Hz) with an Axon instruments 1440A (Molecular Devices) using Clampex 10 software. Setting the Clampex averaging feature to retain all the elements of an average, the 280 ERGs within a single spectral dataset were captured in a single file.

Analysis of ERG signals

Datasets were imported into Origin analysis software and processed using Origin LabTalk scripts (Origin, various versions; Originlab Corporation). The 4 replicate-waveforms at each of the 70 wavelength and irradiance combinations were averaged and boxcar filtered (17 ms, one 60 Hz line-frequency cycle). Peak-to-trough amplitudes were extracted during the 850 ms following stimulus onset, an interval including both the hyperpolarizing trough and repolarizing peak of the Aspartate-isolated cone-PIII response. There was no b-wave component in this signal (Nelson and Singla, 2009). Each amplitude was associated in Origin with the wavelengths and irradiances of the stimuli, providing 70 wavelength, irradiance, and amplitude data points for each spectral dataset. Datasets with unstable response amplitudes over the collection period were rejected. For each genetic variant, multiple datasets from ~10 eyes were normalized to the maximal response in each to form a cumulative datset, and fit to a spectral algorithm. The normalization weighted the individual datasets making up the cumulative dataset equally. Combining datasets from many eyes separates the trends in genetic alterations of spectral properties from the variations among individual eyes. Non-linear fits of models to spectral datasets used the Levenberg-Marquardt iteration algorithm provided by Origin, which extracts amplitudes of various cone signals together with standard errors of estimate (SEs) for statistical comparisons.

Statistical analysis

We use *t*-tests, *F*-tests and ANOVAs to compare results from different treatments or measurements. To determine the most appropriate spectral models, *F*-tests on residual variances for different spectral models were employed. For statistical tests Graphpad Prism software, web-based calculators, and statistical functions addressable within Originlabs Labtalk software were used.

Finding the cone combinations responsible for spectral datasets

Eight cone opsins are expressed in zebrafish retina (Chinen et al., 2003). The algorithm to identify the cone signals generating the ERG spectral shape is based on the axiom that the tiny photocurrents of individual cones sum linearly in extracellular space to produce a net extracellular current which, by traveling through extracellular resistivity, generates an ERG photovoltage. We assume individual cone

photocurrents relate to irradiance through Hill functions of exponent 1.0 and semi-saturation irradiance σ (Baylor and Fuortes, 1970) and that σ varies with wavelength in inverse proportion to opsin absorbance. This scheme is represented in figure 2A (Equation 1). V is the net summed photovoltage in the cone ERG (cone PIII) which depends on I the stimulus irradiance in quanta and wl the wavelength. The Vm_i values are non-linear fit values, the maximal or saturation voltages for each of the i cone types. The semi-saturation irradiance for the i_{th} cone is k_i, as evaluated at the i_{th} cone absorbance maximum. The k_i values differ among cone types relative to each other. The relative k_i values, expressed as log(k_i) relative to UV-cone sensitivity are literature values (Nelson et al., 2019) listed in figure 2C. The UV-cone value for log(k) is fit by the algorithm. $A(wlmax_i, wl)$ is absorbance as a function of wavelength (wl) for the i_{th} cone, whose wavelength maximum is $wlmax_i$. The maximum wavelengths are literature values (Nelson et al., 2019). The Dartnall nomogram (Dartnall, 1953) is used as the absorbance function $A(wlmax_i, wl)$. This approximation has the convenience of making opsin absorbance across wavelengths a function of a single variable, $wlmax_i$. The Dartnall nomogram posits that opsin absorbance shape is constant when plotted on a reciprocal wavelength axis. The template nomogram functions derive from suction electrode recordings of cones in *Danio aequipinnatus* (Palacios et al., 1996), a relative of zebrafish (*Danio rerio*). These templates are represented as 8th order polynomials. We use a single template polynomial (Hughes et al., 1998) for all red, green, and blue cones listed in figure 2C, but a separate polynomial for UV cones (Palacios et al., 1996). The resulting absorbance shapes appear in figure 2B. Altogether there are nine parameters fit by the algorithm: eight Vm_i values, and a single k_i value (k_{UV}).

The spectral algorithm (Fig. 2A) sums signals from 8 cone types (Fig. 2B, 2C). These include a UV cone, two blue cones (B1, B2), three green cones (G1, G3, G4) and two red cones (R1, R2). The gene equivalencies of this nomenclature and the functionally measured wavelength peaks appear in figure 2C. The spectral algorithm implies 2^8-1 or 255 unique cone combinations that might best represent an ERG spectral dataset. Each combination is called a model. The best model is chosen based on four constraints: 1) The model iteration must converge. 2) All model Vm_i values must be significantly greater than zero (t-test, $p \leq 0.05$). 3) All Vm_i values must be less than 2.0, so as not to greatly exceed the largest amplitudes in the cumulative datasets. 4) The value of r^2 for the fit must be larger than that of any other model, as determined by the F-test for residual variance. If equivalent models are found (F-test, $p \geq 0.95$), they will be noted. A similar modeling algorithm has been used to determine the cone combinations impinging on larval ganglion cell impulse discharges (Connaughton and Nelson, 2021).

Results

Cone distributions in the larval retinas of wild-type and crx:trβ2 transgenics

Suzuki et al (2013) developed the *crx:mYFP-2A-trβ2* gain-of function transgenic as a rescue line to restore red-cones during a morpholino blockade of native *trβ2* that abolished their formation. In zebrafish the *crx* gene promotor becomes activate at the retinal progenitor stage (~2 dpf) (Shen and Raymond, 2004). The gain-of-function *crx:trβ2* transgene replaces the missing retinal trβ2, but not in the same cell types or at the same developmental stage. In the experiments of Suzuki et al (2013) it was nonetheless effective. Red cones were restored with supernormal density, but there was suppression of green-, blue- and UV-opsin immunoreactive cones (Suzuki et al., 2013).

In figure 3A and 3B the experiment of Suzuki et al (2013) is repeated on *crx:mYFP-2A-trβ2* larvae without morpholino suppression of native *trβ2*. In WT retinas, immunoreactive mosaics of both UV cones (Fig. 3Ai) and red cones (Fig. 3Aiii) stain with opsin antibodies. Superposition of both mosaics (Fig.3Aii) show no opsin overlaps, with each cone type expressing a single opsin. The situation is similar for blue cones, which exist in a mosaic pattern separate from red cones (Figs. 3Aiv, 3Av, 3Avi).

Red cones are denser than WT in the retinas of the *crx:mYFP-2A-trβ2* larvae (Fig. 3B). Based on figures 3A and 3B, the density of red-opsin immunoreactive cones in 6-dpf transgenics (188,000 mm^{-1}) is significantly greater than WT (72,500 mm^{-1}) [$t(10) = 18.0$, $p = 6.0 \times 10^{-9}$]. The density of *crx:trβ2* UV opsin immunoreactive cones (7900 mm^{-1}, Fig. 3Bi) is significantly less than WT (42,000 mm^{-1}, Fig. 3Ai) [$t(6) = 7.0$, $p = 0.00043$)]. One of the three *crx:trβ2* UV cones (Fig. 3Bi) stains for both UV and red opsins (arrowhead, Figs. 3Bi, 3Bii, 3Biii), indicating co-expression of red and UV opsins. The density of *crx:trβ2* blue opsin immunoreactive cones (13,800 mm^{-1}. Fig. 3Biv) is significantly less than WT (30,500 mm^{-1}, Fig. 3Aiv) [$t(6) = 4.7$, $p = 0.0033$)]. Of four transgenic blue cones illustrated (Fig. 3Biv), one is immunoreactive for red opsin (arrowhead, Figs. 3Biv, 3Bv, 3Bvi), evidence for co-expression of red and blue opsins in a single cone. These alterations in densities of cone types resemble findings obtained in the presence of morpholino blockade of native trβ2 (Suzuki et al., 2013) suggesting the *crx:trβ2* transgene alters cone developmental patterns regardless of the activity of the native *trβ2* gene. The difference is the mixed opsin cones, which was not earlier described.

Cone spectral signals from wild-type and crx:trβ2 retinas in larvae and adults

The spectral pattern of cone signals isolated from the ERGs of larval *crx:mYFP-2A-trβ2* eyes parallels the altered cone densities. In larval perfused *in vitro* eyes, cone signals were isolated from the ERG with 20 mM Aspartate medium, which blocks cone synaptic transmission through saturation of glutamatergic receptors of three types: ionotropic cation channels, metabotropic-mediated cation channels, and glutamate-transporter-mediated anionic channels (Grant and Dowling, 1995, 1996; Connaughton and Nelson, 2000). With short and UV wavelength stimulation (410 nm, 330 nm, Fig. 3C), an isolated WT eye responds with substantial signals for three of the brightest stimulus irradiances (green, yellow or red traces) but at these same wavelengths signals from a *crx:trβ2* eye are evident at only for the two brightest irradiances (yellow and red) and are of lesser amplitude than WT (Fig. 3D). Maximal amplitudes were evoked at 490 nm in the WT eye (Fig. 3C), while amplitudes in the *crx:trβ2* eye plateaued at 490, 570, and 650 nm (Fig. 3D).

The spectral differences in cone signals from adult *crx:mYFP-2A-trβ2* and WT eyecups were even more striking than those in larval eyes. In the WT traces, the maximal amplitude occurred at 490 nm (Fig. 4A), whereas the maximal amplitude from a *crx:trβ2* eyecup was seen at 650 nm (Fig. 4B). Amplitudes at 410 nm and 330 nm (Fig. 4B) were greatly reduced as compared to the WT control (Fig. 4A). At these short wavelengths WT signals were more sensitive than in the *crx:trβ2* eyecup, with the dimmer stimuli (gray, and blue traces, Fig. 4A, 4B) evoking deflections in WT, but only overlapping baselines in *crx:trβ2* eyecups.

Wild-type and crx:trβ2 response waveforms in larvae and adults

The *crx:mYFP-2A-trβ2* transgene subtly changes the amplitudes and kinetics of Aspartate-isolated cone signals (cone PIII). In larvae a greater mean amplitude and greater spread of amplitudes were found (Fig. 4C). The mean of maximal peak-to-trough responses in spectral datasets for 10 WT larval eyes was 89.6 ± 8.7 μV (28 datasets, mean and SE), while the mean of maximal amplitudes for 12 *crx:trβ2* eyes was 145.0 ± 18.7 μV (29 datasets). The *crx:trβ2* amplitudes were somewhat larger [$t(55) = 2.65$, $p = 0.0103$), Fig. 4C]. The dispersion of larval amplitudes was also significantly greater for the transgenic [$F(4.77, 28, 27) = 5.6 \times 10^{-5}$, $p = 0.00011$]. But on reaching adulthood, *crx:trβ2* maximal PIII amplitudes became indistinguishable from WT counterparts (Fig. 4C). In 14 WT eyecups the mean of maximum peak-to-trough amplitudes was 34.4 ± 5.1 μV (20 datasets). In 16 *crx:trβ2* eyecups the mean of maximal peak-to-trough amplitudes was 32.4 ± 6.1 μV (21 datasets). The difference was insignificant [$t(38) = 0.248$, $p = 0.806$]. The variance in maximal amplitudes was similar [$F(1.51, 20, 19) = 0.813$, $p = 0.375$]. Lesser

amplitudes occur in adult eyecups than intact larval eyes as photocurrents escape around eyecup edges, whereas the larval eye is an electrically sealed system. Neither larval nor adult *crx:trβ2* amplitude distributions (Fig. 4C) show evidence of amplitude loss, a characteristic associated with retinal degenerations.

'PIII ON trough' is the time interval from stimulus onset to the minimum in the vitreal negative phase of the cone PIII signal. In larvae, PIII-ON-trough latencies for the *crx:mYFP-2A-trβ2* waveforms were similar to WT, but in adults the latency to the PIII ON trough was shorter in the transgenic (Fig. 4D). Response peak and trough timing were measured on the mean waveform for all 280 responses in a spectral dataset. In this average response, noise is minimized and interferes least with determination of extrema timing. For larval eyes the latency to the cone PIII trough for 29 *crx:trβ2* datasets (12 eyes) was 135 ± 6 ms from stimulus onset (mean and SE). The trough time for 28 WT datasets (10 eyes) was 134 ± 5 ms. The WT and transgenic trough times were not significantly different [$t(55) = 0.218$, $p = 0.828$] and the trough-time variances were also similar [$F(1.80, 28, 27) = 0.935$, $p = 0.133$, Fig. 4D]. In 16 adult *crx:trβ2* eyecups the mean latency to PIII ON troughs was 111 ± 3 ms (21 datasets). In 14 WT eyecups the PIII trough latency was 124 ± 5 ms (20 datasets). The adult *crx:trβ2* transgenics were somewhat quicker to peak [$t(39) = 2.133$, $p = 0.039$]. The variances in onset latencies was similar in *crx:trβ2* and WT adults [$F(2.11, 19, 20) = 0.947$, $p = 0.106$, Fig. 4D]. For WT controls, larval and adult trough latencies did not differ significantly [$t(46) = 1.45$, $p = 0.155$]. For *crx:trβ2* transgenics trough times for adults were significantly quicker than for larvae [$t(48) = 3.23$, $p = 0.0022$)].

'PIII OFF peak' (Fig. 4E) is the time interval from stimulus offset to the maximum of the upward course in the PIII OFF signal. The larval PIII-OFF-peak latencies for *crx:mYFP-2A-trβ2* (360 ± 36 ms) did not differ significantly from WT controls [313 ± 17 ms, $t(55) = 1.171$, $p = 0.247$], although the variance in *crx:trβ2* timing was significantly greater [$F(4.68, 28, 27) = 0.999$, $p = 1.3 \times 10^{-4}$]. In adults the *crx:mYFP-2A-trβ2* OFF peak (262 ± 14 ms), like the ON trough, occurred significantly sooner than in WT [329 ± 20 ms, $t(39) = 2.728$, $p = 0.0095$]. The variances of adult OFF-peak latencies were similar in *crx:trβ2* and WT adults [$F(1.99, 19, 20) = 0.932$, $p = 0.135$, Fig. 4E]. For WT controls, larval and adult PIII OFF peak timing was not significantly different [$t(46) = 0.600$, $p = 0.551$]. For *crx:trβ2* transgenics PIII-OFF-peak times for adults were somewhat quicker than for larvae [$t(48) = 2.234$, $p = 0.030$]. Taken together the latency distributions (Fig. 4D, 4E) show little evidence of waveform abnormalities associated with errors in cone phototransduction or retinal disease. The quicker waveforms of *crx:trβ2* adults may result from different weighting of contributing cone types.

In crx:trβ2 larvae, red-cone signals increase but UV- and blue-cone signals diminish

Inspection of differences in larval signal amplitudes across the stimulus spectrum (Fig. 3C, 3D) suggests that the complement of cone types contributing to vitreal cone-PIII signals is altered by the *crx:mYFP-2A-trβ2* transgene. To determine the cone contributions affected, 255 models comprising all combinations of 8 cone spectral types, the latter, a number determined from molecular and physiological approaches (Chinen et al., 2003; Mackin et al., 2019; Nelson et al., 2019), were fit to *crx:trβ2* and WT cumulative spectral datasets. For WT larvae, the cumulative dataset included 1858 response amplitudes (28 datasets), and for *crx:trβ2* larvae there were 1860 such stimuli (29 datasets). The optimal models differed (WT, #111; *crx:trβ2,* #202). The residual variance of the WT model (#111) as fit to the *crx:trβ2* cumulative dataset differed from the residual variance of the *crx:trβ2* dataset fit to optimal model #202 [$F(9.16,1821,1825) = 1$, $p < 0.00001$], indicating that the WT model is not an equivalently good representation of *crx:trβ2* data.

In figures 5A and 5B, amplitudes are plotted against irradiance for four of the 9 test wavelengths. Continuous curves are calculated from the optimal models for WT and *crx:mYFP-2A-trβ2* datasets. These curves are generated from a global model fit to all spectral data. The adherence of irradiance-response curves to datapoints for individual wavelengths is an index of the ability of the global model to represent the cumulative spectral data. The distribution of points and curves is more compressed along the irradiance axis for *crx:trβ2* larvae (Fig. 5B) than for WT controls (Fig. 5A). The points and curve at 370 nm (magenta) lie to the left of the 490 nm points and curve (green) for WT spectral signals (Fig. 5A) but to the right of the 490 nm curve and points for *crx:trβ2* larvae (Fig. 5B), suggesting a loss of sensitivity for 370-nm-sensing cones (UV cones). The log of semi-saturation irradiance calculated for the R1 and R2 cones was 4.56 ± 0.018 for WT larvae and 4.53 ± 0.027 for *crx:trβ2* (Fig. 5A, 5B). These semi-saturation irradiances did not significantly differ [$t(3681) = 1.858$, $p = 0.063$].

The inferred Vm_i values for individual larval cone types (Fig. 2, Eq. 1) relate closely to their functional strength in the cone-PIII signal. In figure 5C the modeled values are compared for WT and *crx:mYFP-2A-trβ2* larvae. Six cone types significantly contributed to WT cone-PIII signals (Vu358-UV, Vb415-B1, Vb440-B2, Vg460-G1, Vg500-G4, Vr556-R2), but only four cone contributions were identified in *crx:trβ2* larvae (Vb415-B1, Vg460-G1, Vr556-R2, Vr575-R1). Missing in the transgenic are UV cone signals (Vu358), B2 cone signals (Vb440), and G4 signals (Vg500). But an extra red-cone signal, R1 (Vr575), not detected in WT, became significant in *crx:trβ2* larvae [$t(1825) = 2.715$, $p = 0.0067$]. The R2 (Vr556) cone signal in this 6-dpf dataset did not differ from WT [$t(3647) = 0.318$, $p = 0.751$], nor did either the B1 signal (Vb415) [$t(3647) = 0.96$, $p = 0.338$] or the G1 signal (Vg460) [$t(3647) = 1.868$, $p = 0.062$]. Overall, the modeling algorithm shows that UV-cone amplitudes were lost, red-cone amplitudes increased, and among four blue and green cones signals, two were lost and two were unaffected.

Modeled spectral sensitivities represent the impact of both Vm_i and k_i values and include Hill-function response compressions, which flatten cone spectral functions for bright stimulation (Eq.1, Fig. 2A). This is the fullest model representation, but less interpretable in terms of individual cone contributions. The spectral curves of figure 5D are modeled response amplitudes for three levels of constant quantal stimulation across the spectrum. The strong UV signal in WT larval eyes (Fig. 5A) appears as an ultraviolet spectral peak (~370 nm) in figure 5D, regardless of stimulus brightness, despite the larger saturation amplitudes of the R2 (Vr556) cones, which, in WT controls, manifest as a long-wavelength bulge prominent with greater constant-quantal irradiances, which better stimulate the higher semi-saturation characteristics of R2 physiology. The failure to find UV cone signals in the *crx:trβ2* larval transgenics precludes an ultraviolet peak at any quantal-irradiance and allows red-cone signals to create spectral peaks (540-550 nm). The residual blue and green signals of *crx:trβ2* cooperate to create a 444 nm peak at the dimmest level of stimulation (Fig. 5D).

With 255 models tested, there is not always a single best-fitting model for each dataset as judged by residual variance. For the larval WT datasets, model #95, also a 6-cone model, was indistinguishable from model #111 [$F(0.99895, 1851, 1851) = 0.491$, $p = 0.982$]. This model replaces the G4 (Vg500) cone signal with a G3 (Vg480) signal. The WT five-cone model #103 was also indistinguishable [$F(0.99719, 1851, 1852) = 0.476$, $p = 0.952$]. This model omits the low-amplitude G1 (Vg460) cone signal. For the *crx:trβ2* datasets, model 201 was indistinguishable from model 202 [$F(0.999, 1856,1856) = 0.491$, $p = 0.9822$]. This model substitutes a low-amplitude UV-cone signal (Vu358) for the low-amplitude B1-cone signal (Vb415).

Adult crx:trβ2 zebrafish are red cone dichromats

Only the red R1 (Vr575) and R2 (Vr556) cone signals make significant contributions to the adult cone-PIII responses of *crx:mYFP-2A-trβ2* (Fig. 6C). A five-cone model including blue-, green- and red-cones

best represent WT adult controls (Vb415-B1, Vg460-G1, Vg500-G4, Vr556-R2, Vr575-R1). The cumulative datasets included 14 eyecups from WT adults and 16 from *crx:trβ2* adults (WT, 20 datasets, 1400 responses; *crx:trβ2*, 21 datasets, 1470 responses). When the adult WT model (#234) is fit to the adult *crx:trβ2* dataset, the residual variance is larger than the optimal *crx:trβ2* model variance (#192) [$F(1.923,1443,1445) = 1$, $p < 0.0001$] indicating different spectral patterns are operating. The *crx:trβ2* transgene alters the positioning of both irradiance-response data points and model curves (Figs. 6A, 6B). The 370 and 490 nm curves and points (magenta and green) lie to the left side of the 570 nm curve and points (yellow) in WT adults, but shift to the right side of the 570 nm curve and points in *crx:trβ2* adults, a diminution of UV- and mid-wavelength sensitivity. The calculated log of semi-saturation irradiance for long-wavelength-sensitive cones (R1, R2) was 4.49 ± 0.033 for WT adults and 4.69 ± 0.022 for *crx:trβ2* adults (Fig. 6A, 6B), *crx:trβ2* being significantly less sensitive [$t(2818) = 5.17$, $p = 2.5 \times 10^{-7}$]. The modeled amplitudes of cones with significant signals appear in Fig. 6C. In the adult WT model, blue- and green- cone signals are detected, but these signals are not evident in adult *crx:trβ2* transgenics, where there are only red-cone signals. In *crx:trβ2*, R1 cones contribute a significantly larger amplitude signal than R2 cones [180%, $t(2818) = 3.92$, $p = 0.000092$)], whereas in the WT controls, R1 and R2 signal amplitudes were not significantly different [$t(2818) = 0.782$, $p = 0.434$].

The modeled spectral curves for the *crx:mYFP-2A-trβ2* adult red-cone dichromat (Fig. 6D) show long-wavelength-peaking functions at 565 nm at all quantal stimulation levels, while WT spectral peaks occur between 430 nm and 522 nm, depending on stimulus brightness. Except at wavelengths greater than 570 nm, WT control amplitudes are greater than transgenic, due both to the greater sensitivity of WT cones overall, and to the presence of mid- and short-wavelength (blue and green) cones, absent in the transgenic. As judged by residual variance no other models were indistinguishable from the illustrated ones for either *crx:trβ2* or WT adults (F-tests for all other models, $p < 0.95$).

Cone types and spectral signals in larval gnat2:trβ2 retinas

The *gnat2:mYFP-2A-trβ2;mpv17* transgenic was developed to test whether red-cones could be restored to a population of cones already differentiated under morpholino blockade of the native *trβ2* gene, which prevented red-cone development (Suzuki et al., 2013). The *gnat2* locus codes for cone transducin α, a gene product only expressed in differentiated and functional cone cells. It is expressed by 4 dpf. Suzuki et al (2013) found the *gnat2:trβ2* transgene induced a supra-normal 5-dpf density of red-opsin immunoreactive cones in the absence of native trβ2, but unlike the *crx:mYFP-2A-trβ2* rescue, green- (RH2), blue- (SWS2) and UV- (SWS1) opsin immunoreactive cone densities were normal (Suzuki et al., 2013).

A similar pattern of larval opsin immunoreactivity is seen in the absence of morpholino blockade of native trβ2. In the control retina (*roy orbison mpv17*$^{-/-}$) both UV and red cones (Fig. 7Ai, 7Aiii) stain with opsin antibodies. Superposition of red- and UV-cone mosaics (Fig.7Aii) shows no red- and UV- opsin overlap, with each opsin expressed in a separate cone cell. The control larval blue cones also exist in a mosaic pattern separate from red cones (Figs. 7Aiv, 7Av, 7Avi). The *gnat2:trβ2* retina shows dense representations of UV- and blue-opsin-immunoreactive cones (Figs. 7Bi, 7Biv). Red-opsin immunoreactive cones appear denser in *gnat2:trβ2* than in *mpv17*$^{-/-}$ control retinas (Figs. 7Biii, 7Bvi). The *gnat2:trβ2* red cone density (95,500 mm^{-1}) is significantly greater than the control strain (51,400 mm^{-1}) [$t(14)=6.7$, $p = 0.000011$, Figs. 7Aiii, 7Avi, 7Biii, 7Bvi]. The densities of UV- and blue-opsin immunoreactive cones were similar in *gnat2:trβ2* and controls. The *gnat2:trβ2* UV-cone density (34,252 mm^{-1}) was not significantly different from *mpv17*$^{-/-}$ (23,435 mm^{-1}) [$t(6)=1.7$, $p = 0.143$], nor was the *gnat2:trβ2* blue-cone density (21,633 mm^{-1}) different from *mpv17*$^{-/-}$ (27,041 mm^{-1}) [$t(6)=1.6$, $p = 0.168$].

In these 12-dpf *gnat2:trβ2* transgenics (Fig. 7B), UV- and blue-opsin immunoreactive cones were frequently immunoreactive for red opsins (arrowheads), with 2/3 of cones being mixed opsin types.

Densities of cone types and mixed opsin patterns were similar earlier in development. At 7 dpf, the density of red-opsin immunoreactive cones in the was 70,800 mm^{-1}, significantly greater than the *mpv17*$^{-/-}$ control (52,300 mm^{-1}) [$t(10)=13.0$, $p = 1.3 \times 10^{-7}$]. The densities of blue-opsin immunoreactive cones were similar [*gnat2:trβ2,* 22,000 mm^{-1}; *mpv17*$^{-/-}$, 24,900 mm^{-1}, $t(7)=1.9$, $p = 0.096$], but the density of 7-dpf *gnat2:trβ2* UV immunoreactive cones was slightly less [*gnat2:trβ2,* 36,900 mm^{-1}; *mpv17*$^{-/-}$, 46,900 mm^{-1}, $t(8)=3.4$, $p = 0.010$]. Mixed blue-red and UV-red opsin expression was noted in about 10% of 7-dpf blue- or UV- opsin immunoreactive cones.

Larval and adult cone spectral signals from control and gnat2:trβ2 retinas

Despite greater red-cone density and numerous mixed opsin cones (Fig. 7B), the spectral patterns of larval, Aspartate-isolated cone signals (cone-PIII) from in-vitro *gnat2:mYFP-2A-trβ2;mpv17*$^{-/-}$ eyes are similar to the *mpv17*$^{-/-}$ controls. In the trace recordings of figure 7C, an *mpv17*$^{-/-}$ control larval eye produces substantial signals at all wavelengths, with maximal amplitudes for the 490 nm stimulus. A *gnat2:trβ2* larval eye gives a similar amplitude pattern for the test wavelengths and irradiances (Fig. 7D), with maximal amplitudes at 490 nm.

In an adult *mpv17*$^{-/-}$ control eyecup (Fig. 8C), the spectral pattern of cone-PIII ERG waveforms resembles those of larvae, with a broad range of responsiveness across wavelengths, and the 490-nm stimuli yielding an amplitude peak. An adult *gnat2:mYFP-2A-trβ2;mpv17*$^{-/-}$ eyecup also shows a broadly responsive spectral pattern (Fig. 8B), but greater amplitudes are evoked at long wavelengths (570 nm, 650 nm), suggesting that the underlying input signals from red, green, blue and UV cone types have undergone developmental transformation.

Similar waveforms from control and gnat2:trβ2 larvae and adults

There was little difference in the distribution of amplitudes or waveform kinetics between *gnat2:mYFP-2A-trβ2;mpv17*$^{-/-}$ transgenic and the *mpv17*$^{-/-}$ control strain (Figs. 8C, 8D, 8E). In both larvae and adults, the maximal ERG PIII amplitudes were similar for the *gnat2:trβ2* transgenics and controls. The larval mean of dataset-maximum peak-to-trough responses (23 datasets, 15 eyes, 6 dpf) for *mpv17*$^{-/-}$ controls was 110.5 ± 12.1 μV (mean and SE). For *gnat2:trβ2* larvae, the mean of dataset-maximum peak-to-trough amplitudes was 130.3 ± 16.5 μV (22 datasets, 17 eyes, 6 dpf). Maximal amplitudes of the larval *gnat2:trβ2* signals were not significantly different from those of the background strain [$t(43) = 0.969$, $p = 0.338$)]. The variances in maximal dataset amplitudes were similar in transgenic and control larvae [$F(1.79, 21, 22) = 0.908$, $p = 0.185$].

Adult *gnat2:mYFP-2A-trβ2;mpv17*$^{-/-}$ maximal cone PIII amplitudes were not distinguishable from controls (Fig. 8C). In 16 *mpv17*$^{-/-}$ adult eyecups the mean of dataset-maximum peak-to-trough amplitudes was 22.5 ± 3.1 μV (30 datasets). In 15 *gnat2:trβ2* eyecups the mean of dataset-maximum peak-to-trough amplitudes was 28.2 ± 7.2 μV (24 datasets). The difference was not significant [$t(52) = 0.780$, $p = 0.439$]. The variance in adult transgenic peak amplitudes was greater [$F(4.38, 23, 29) = 0.9999$, $p = 0.00025$].

Examining kinetics of the larval and adult dataset mean waveforms, the latency to the cone-PIII trough minimum and the variance in its timing differed little between larval *gnat2:trβ2* eyes and the *mpv17*$^{-/-}$ controls (Fig. 8D). The onset time for the larval cone-PIII trough for *gnat2:trβ2* eyes (29 datasets, 17 eyes) was 152 ± 5 ms from stimulus onset (mean and SE). The cone-PIII trough latency for larval eyes from the *mpv17*$^{-/-}$ controls (26 datasets, 16 eyes) was 139 ± 4 ms. The trend, though not significant, for larval *gnat2:trβ2* onset kinetics was towards greater delay in the PIII ON trough [$t(53) = 1.89$, $p =$

0.065)]. Larval *gnat2:trβ2* eyes trended, though not significantly, towards greater variability in trough latencies [$F(2.09, 28, 25) = 0.9669$, $p = 0.067$].

For adults the mean time to the PIII ON trough was 122 ± 4 ms in *gnat2:trβ2* eyecups (24 datasets, 15 eyes) and 128 ± 4 ms in the *mpv17*$^{-/-}$ controls (26 datasets, 16 eyes). The differences were not significant [$t(48) = 1.11$, $p = 0.274$)]. The variances in adult trough latencies for *gnat2:trβ2* and background strain were similar [$F(1.23, 25, 23) = 0.689$, $p = 0.623$]. Adult trough latencies were significantly quicker than larvae for both *mpv17*$^{-/-}$ controls and *gnat2:trβ2* transgenics [*mpv17*$^{-/-}$: $t(50) = 2.03$, $p = 0.047$; *gnat2:trβ2* $t(51) = 4.39$, $p = 0.000057$].

The mean timing and variance in larval and adult *gnat2:mYFP-2A-trβ2 mpv17*$^{-/-}$ cone-PIII OFF peaks did not differ from background strains (Fig. 8E). In the mean waveforms for the larval datasets, the *gnat2:trβ2* light-OFF peak occurred 321 ± 22 ms after stimulus offset (29 datasets, 15 eyes). For the larval *mpv17*$^{-/-}$ background strain, the OFF peak occurred at 292 ± 18 ms (26 datasets, 16 eyes). These latencies were not significantly different [$t(53) = 0.980$, $p = 0.332$]. The variances in larval OFF peak timing for transgenic and control were similar [$F(1.83, 28, 25) = 0.935$, $p = 0.132$]. For adult datasets, the OFF peak of mean waveforms from *gnat2:trβ2* gave delays of 308 ± 17 ms from stimulus offset (24 datasets, 15 eyes). In the adult *mpv17*$^{-/-}$ control datasets, the delay was 309 ± 14 ms. The adult OFF-peak timing did not differ between transgenic and control [$t(48) = 0.031$, $p = 0.976$)]. The variances in adult OFF peak timing were not different [$F(1.34, 23, 25) = 0.763$, $p = 0.473$]. Adult OFF-peak latencies did not differ significantly from larvae for either *mpv17*$^{-/-}$ controls or *gnat2:trβ2* transgenics [*mpv17*$^{-/-}$: $t(50) = 0.75$, $p = 0.459$; *gnat2:trβ2*: $t(51) = 0.43$, $p = 0.670$]. Overall, the *gnat2:trβ2* transgene has little effect on cone-PIII amplitudes or waveforms. There is no electrical evidence of degenerative disease.

In larvae the gnat2:trβ2 transgene increases R2-cone signals

The larval cone PIII spectral response amplitudes of *gnat2:mYFP-2A-trβ2;mpv17*$^{-/-}$ seem similar to the *mpv17*$^{-/-}$ control strain (Fig. 7C, 7D). Signal loss in the UV and signal gain at long wavelengths, as seen *crx:mYFP-2A-trβ2* larvae (Figs. 3C, 3D), are not evident by inspection. But modeling of data suggests the cone signals in the two larval cohorts differ. The optimal model for *gnat2:trβ2* is #79, and optimal control model is #77. Applying the control model #77 to the *gnat2:trβ2* dataset gives a greater residual variance than the optimal model #79 [$F(1.21, 1506, 1511) = 0.999$, $p = .00021$], indicating that cone inputs generating the *gnat2:trβ2* dataset differ from control. In figures 9A and 9B, amplitudes are plotted against irradiance for four of the 9 test wavelengths and compared to continuous curves calculated from best-fitting models. These are fit to 1945 points (15 eyes, 28 spectral datasets) for *mpv17*$^{-/-}$ controls and 1540 points (17 eyes, 22 spectral datasets) for *gnat2:trβ2*. The distribution of points and curves at 570, 490 and 370 nm are more overlapping along the irradiance axis for *gnat2:trβ2* larvae than are the same wavelength points and curves for the control strain. Points and curves at 370 and 490 nm (magenta, green) lay to the left of the 570 nm points and curve (yellow) for *mpv17*$^{-/-}$ controls but coincide with the 570-nm curve for *gnat2:trβ2*, suggesting less sensitivity from short- and mid-wavelength-sensitive cones. The logs of semi-saturation irradiances for the red (R1, R2) cones were 4.50 ± 0.02 for *mpv17*$^{-/-}$ larvae and 4.51 ± 0.02 for *gnat2:mYFP-2A-trβ2;mpv17*$^{-/-}$ (Fig. 9A, 9B), nearly identical [$t(3422) = 0.251$, $p = 0.802$)].

Four cone signals are identified in larval *mpv17*$^{-/-}$ controls, but five were found in *gnat2:mYFP-2A-trβ2* siblings (Fig. 9C). Significantly reduced in *gnat2:trβ2* are UV and B2 cone amplitudes [Vu358: $t(3422) = 5.36$, $p = 8.7 \times 10^{-8}$; Vb440: $t(3422) = 2.65$, $p = 0.0081$]. Significantly increased are B1and R2 cone signals [Vb415: $t(1511) = 2.90$, $p = 0.0038$; Vr556: $t(3422) = 9.94$, $p = 5.6 \times 10^{-23}$)]. The G1 cone signal was not significantly affected [Vg460, $t(3422) = 0.851$, $p = 0.395$]. The larval *mpv17*$^{-/-}$ control and

gnat2:trβ2 model-generated spectral sensitivities are similar (Fig. 9D), but with increased long-wavelength and decreased short-wavelength sensitivities in *gnat2:trβ2*. This leads to long-wavelength spectral peaks between 535 nm and 549 nm for *gnat2:trβ2*, not seen in the *mpv17*$^{-/-}$ controls. While there is a definite spectral shift towards long-wavelength sensitivity in *gnat2:trβ2* larvae, the extent is less than seen in *crx:trβ2* larvae (Fig. 5D).

Of the 255 models fit to the larval *gnat2:trβ2* combined datasets none were deemed to fit equally as well as model #79 based on residual variance, that is by an *F*-test with $p \geq 0.95$. Two were indistinguishable from the best-fit model 77 for the *mpv17*$^{-/-}$ controls. Model 103 [$F(0.9992, 1939, 1940) = 0.493$, $p = 0.986$], employed an additional 5th cone substituting G4 for G1 and adding B1. Model 101 [$F(0.9972, 1940, 1940) = 0.475$, $p = 0.95$] substituted G4 for G1. All three indistinguishable control models agreed on the presence of UV, B2 and R2 cone signals in *mpv17*$^{-/-}$ controls.

Adult gnat2:trβ2 retinas generate large R1 red-cone signals

In the adult *gnat2:mYFP-2A-trβ2;mpv17*$^{-/-}$ eyecup (Fig. 8B), large-amplitude responses to 570- and 650-nm stimuli suggest an increased contribution of red-cones as compared to either *gnat2:trβ2* larvae (Fig. 7B) or adult controls (Fig. 8A). To determine the cone-type composition of adult *gnat2:trβ2* retinal cone signals we searched for the best models to represent the *gnat2:trβ2* cumulative spectral dataset. Trough-to-peak amplitudes for all eyes and datasets (*mpv17*$^{-/-}$, 13 eyes, 23 datasets, 1610 responses; *gnat2:trβ2*, 11 eyes, 20 datasets, 1400 responses) were fit to the 255 combinations of 8 cones. Model #219 fit best for *mpv17*$^{-/-}$ control eyecups, and model #202, for *gnat2:trβ2*. When the adult *gnat2:trβ2* cumulative dataset was fit to the control model #202, the residual variance was significantly greater, indicating the spectral properties of the *gnat2:trβ2* gain-of-function dataset differed significantly from the control [$F(1.942, 1370, 1374) = 1$, $p < .00001$].

For both points and optimal model curves the *gnat2:trβ2* transgene alters adult irradiance-response characteristics (Fig. 10). In the control dataset (*mpv17*$^{-/-}$), the 570 nm points and curve (yellow) show less sensitivity than either the 370 or 490 nm points and curves (magenta, green), but greater sensitivity in the *gnat2:trβ2* (Figs. 10A, 10B). In *gnat2:trβ2*, brighter stimuli are required to elicit responses in the UV (370 nm) and mid spectrum (490 nm). The fit of log of semi-saturation irradiances for the red cones (R1, R2) were 4.30 ± 0.026 for adult controls and 4.43 ± 0.026 for *gnat2:trβ2* adults (Figs. 10A, 10B), a significantly greater sensitivity (~35%) than for *gnat2:trβ2* adults [$t(2953) = 3.44$, $p = 0.0006$)].

In the best-fitting model for *gnat2:mYFP-2A-trβ2;mpv17*$^{-/-}$ adults, the long-wavelength R1 cone (Vr575) contributes the largest amplitude signal with the R2 amplitude (Vr556) being 22% of the R1 amplitude, significantly less than R1 [$t(2748) = 5.23$, $p = 2.6 \times 10^{-17}$)], and only marginally different from zero [$t(1375) = 2.02$, $p = 0.044$), Fig. 10C]. In the *mpv17*$^{-/-}$ control, both R1 and R2 red cone amplitudes were highly significant [Vr575-R1, $t(1580) = 6.01$, $p = 4.1 \times 10^{-18}$; Vr556-R2, $t(1580) = 5.52$, $p = 8.0 \times 10^{-17}$] and did not significantly differ in amplitude [$t(3158) = 0.042$, $p = 0.966$), Fig. 10C]. A six-cone model best fit adult control datasets (Vu358-UV, Vb415-B1, Vg460-G1, Vg480-G3, Vr556-R2, Vr575-R1). A four-cone model sufficed for *gnat2:trβ2* adults (Vb415-B1, Vg460-G1, Vr556-R2, Vr575-R1). Unlike larvae (Fig. 9C) no UV-cone signals were detected in *gnat2:trβ2* adults (Fig. 10C).

At all levels of constant quantal stimulation long-wavelength spectral peaks between 560 and 570 nm are modeled for *gnat2:mYFP-2A-trβ2;mpv17*$^{-/-}$ (Fig. 10D). Models of the *mpv17*$^{-/-}$ control peak between 441 and 493 nm depending on stimulus brightness. Except at wavelengths greater than 540 nm, control amplitudes were greater than transgenic, due both to the greater cone sensitivities (lesser half-saturation irradiances), and to the significantly greater amplitudes of numerous mid- and short-wavelength cones (Vu358-UV, Vb415-B1, Vg460-G1, Vg480-G3).

As judged by residual variance no models were indistinguishable from the illustrated ones for *gnat2:mYFP-2A-trβ2*;*mpv17*$^{-/-}$ adults (*F*-tests for other models, $p < 0.95$). Model #235 was indistinguishable from model #219 (the best model) for the *mpv17*$^{-/-}$ control adults [$F(0.9978, 1603, 1603) = 0.482$, $p = 0.96$]. Models #235 and #219 both employed 6 cones, but model #235 substituted the G4 (Vg500) for the G3 (Vg480) cone.

Properties of the larval dual opsin UV cone in gnat2:trβ2 transgenics

Many cones in *gnat2:mYFP-2A-trβ2;mpv17*$^{-/-}$ larvae express mixed opsins, overlaying a red opsin on the native expression of a shorter-wavelength opsin (Fig. 7B). A few dual-opsin cones also occur in *crx:mYFP-2A-trβ2* larvae (Fig. 3B). The spectral physiology of such cones is of interest. The wide spectral separation of red and UV opsins makes red opsin signals in UV cones amenable to electrophysiological study. The developmental course of mixed opsin cones is also of interest. One proposal is that zebrafish transgenic dual-opsin cones are analogous to the stable *mws-sws* cone configuration seen in rodents (Jacobs et al., 1991; Applebury et al., 2000; Suzuki et al., 2013). Another proposal is that the mixed-opsin cones in *gnat2:trβ2* zebrafish are transitional states, later to develop into red cones. The tendency to lose UV opsin signals in trβ2 gain-of-function transgenics suggests an adverse action on UV cones.

To observe the effects of excess trβ2 on *sws1* (UV opsin) gene expression, UV opsin immunoreactivity was examined in double transgenic *gnat2:trβ2* larvae to which a fluorescent *sws1* opsin reporter gene was added (*gnat2:mYFP-2A-trβ2*;*sws1:nfsBmCherry*;*mpv17*$^{-/-}$). Confocal micrographs of tangential planes through the cone photoreceptor layers in control and the double transgenic larvae appear in figure 11. For the *mpv17*$^{-/-}$ control, all UV-opsin immunoreactive cones (green) express the *sws1:nfsBmCherry* UV-opsin gene reporter as a magenta cytoplasmic halo surrounding the narrower bright green immunofluorescence of the UV-cone outer segment (Fig. 11A). UV and red opsin immunoreactivities are segregated, being expressed in separate cone cells (Figs. 11B, 11C, 11D), the native larval opsin expression pattern (Allison et al., 2010). In the larval *gnat2:trβ2* double transgenic not all UV-opsin immunoreactive cones show the magenta halo of the *sws1:nfsBmCherry* reporter gene (Fig. 11E). In some, the *sws1* reporter gene generates no fluorescence, suggesting the native *sws1* locus is inactive, and UV-opsin, while still present, is no longer being synthesized. Only legacy immunoreactivity remains. In figures 11F-11H patterns of immunoreactivity for UV-opsin and red-opsin are compared. The arrowheads point to cone cells where both UV and red opsin are co-expressed. A comparison of figure 11F with figure 11E reveals that UV-opsin immunoreactive cones with inactive *sws1* reporter genes are the same cones that are double immunoreactive for both UV- and red- opsins (Fig. 11E, checkered arrowheads). The expression of red opsin in a UV cone by the gain-of-function *gnat2:trβ2* transgene appears incompatible with continued expression of UV-opsin, suggesting that the presence of gain-of-function trβ2 either directly or indirectly blocks the *sws1* gene. Therefore, co-expression of UV- and red- opsin immunoreactivity cannot continue indefinitely, as in rodents, but would be limited by the catabolism of previously expressed, but not renewed, UV-opsin.

At the same developmental stage (5 dpf), the functional properties of UV-cones with co-expression of red opsin were explored. In this earliest embryonic dataset, the same 5-cone model (#79) was the best fit for both control and *gnat2:trβ2* gain-of-function larvae (Fig. 11-I), and the residual variance of the *gnat2:trβ2* dataset was not significantly greater when modeled with the control amplitude distribution [$F(1.031,1230,1235) = 0.705$, $p = 0.591$], although the R2-cone saturation amplitude (Vr556) trended greater in *gnat2:trβ2* [$t(3091) = 3.39$, $p = 0.0007$)], a pattern consistent with later developmental stages. Saturation amplitudes of the shorter-wavelength cone signals in *gnat2:trβ2* and control were indistinguishable [Vu358: $t(3091) = 0.56$, $p = 0.57$); Vb415: $t(3091) = 0.25$, $p = 0.81$); Vb440: $t(3091) =$

1.05, $p = 0.29$); Vg460: $t(3091) = 0.084$, $p = 0.93$)]. UV-cone saturation amplitude at 5 dpf appeared unaffected by numerous of its members both lacking *sws1* gene activity and co-expressing red opsin.

Red chromatic adaptation should desensitize UV/red mixed opsin cones to UV stimulation. 650-nm red stimuli do not affect UV opsins, but 370-nm UV stimuli are strongly absorbed. We generated irradiance-response functions at 650 nm and 370 nm in the presence of red or IR backgrounds (Figs. 11J, 11K). For the *mpv17*$^{-/-}$ control, irradiance-response curves for 370-nm stimuli overlap in both datapoints and Hill-function curve fits regardless of background illumination (Fig. 11J). Hill function fits give semi-saturation values of 4.53 log(quanta·μm^{-2}·s^{-1}) for the IR background and 4.59 for the 627-nm background, not distinguishable [$t(290) = 1.26$, $p = 0.210$)], an expected result as UV-opsin does not absorb the 627-nm adapting light. As the 650-nm stimuli (Fig. 11J) are not as efficiently transduced, even by red cones, the 650-nm irradiance-response functions shift to greater irradiances. On the IR background the 650-nm semi-saturation irradiance is 6.38 log(quanta·μm-^{2}·s^{-1}) but increases to 6.53 log(quanta·μm-^{2}·s^{-1}) with the 627-nm background, a significant desensitization [$t(583) = 3.66$, $p = 0.0003$)]. The absorption of the red background by the red-cone red opsin reduces red-cone sensitivity (Fig. 11J).

What was unexpected was that the 370-nm irradiance functions for the *gnat2:trβ2* gain-of-function larvae, with co-expression of red opsin in some UV cones, were unaffected by the red background (Fig. 11K). The red opsin in the mixed-opsin UV cones, which would be activated by the 627-nm background, does not desensitize 370-nm UV signals. For 370-nm stimuli, Hill fits give semi-saturation irradiances of 4.42 log(quanta·μm-^{2}·s^{-1}) on the IR background and 4.44 log(quanta·μm-^{2}·s^{-1}) on the 627-nm background, values not significantly different [$t(205) = 0.300$, $p = 0.765$)]. But the same red background significantly desensitizes red-opsin signals from *gnat2:trβ2* red cones, as seen with 650-nm stimuli (Fig. 11K). The Hill semi-saturation changed from 6.26 log(quanta·μm^{-2}·s^{-1}) on the IR background to 6.55 log(quanta·μm^{2}·s^{-1}) on the 627-nm background, a significant increase [$t(415) = 5.01$, $p = 1.5\times 10^{-12}$], which demonstrates the effectiveness of this background for red opsins (Fig. 11K). The failure of long-wavelength backgrounds to affect UV signals from mixed-opsin cones has also been observed in ERG spectra of rodents (Jacobs et al., 1991). In zebrafish the spectral physiology of UV cones appear, at least early in development at 5 dpf, not to be affected by the introduction of transgenic red opsins in many UV-cone members.

Thyroxin receptor β2 gain-of-function transgenes alter cone morphology

Thyroid hormone receptor β2 is required in zebrafish for both the development of red cones and the expression of red opsins (Deveau et al., 2020). Morphologically, adult red cones are the principal members of zebrafish double cones (Engstrom, 1960; Raymond et al., 1993). Double cones failed to develop in *trβ2*$^{-/-}$ mutants (Deveau et al., 2020). The impact of trβ2 in determining the course of cone morphological development is seen in transverse optical sections of individual transgenic cones from *in vivo* 6-dpf larvae (Fig. 12). These are higher magnifications taken from larval retina confocal image stacks as in figures 1D, 1E and 1F. On inspection, the fluorescent-reporter shapes of trβ2 gain-of-function cones are distinct from the control morphologies of red, blue and UV cones, the latter marked by the reporter fluorescent proteins expressed in *sws2:GFP* (UV cones) and *sws1:GFP;trβ2:tdTomato* (blue and red cones) (Fig. 1D, 12A, 12C).

The maximal widths of the five sorts of cone inner segments illustrated differ [ANOVA, $F(4, 356) = 36.98$, $p < 0.00001$]. The maximal widths for cone inner segments of *crx:mYFP-2A-trβ2* labeled cones are significantly wider than red cones (*post-hoc Tukey*, $p < 0.000001$), as are the maximal widths of cone inner segments of *gnat2:mYFP-2A-trβ2*;*mpv17*$^{-/-}$ labeled cones (*post-hoc Tukey*, $p = .00024$). Neither trβ2 gain-of-function cone is as wide as the inner segments of UV cones (*post-hoc Tukey*: *crx:mYFP-2A-trβ2,*

$p = 0.00005$; *gnat2:mYFP-2A-trβ2;mpv17*$^{-/-}$, $p < 0.000001$). The inner segment widths of the *crx:mYFP-2A-trβ2* cones were not distinguishable from blue cones (*post-hoc Tukey*: $p = 0.126$), while *gnat2:mYFP-2A-trβ2* widths were marginally narrower than blue cones (*post-hoc Tukey*: $p = 0.00764$).

The lengths of axons between the base of cone inner segments and the apex of cone synaptic pedicles differ among the cone types illustrated in figure 12C [ANOVA, $F(4, 290) = 9.692$, $p < 0.00001$]. In the trβ2 gain-of-function cones, the length of the axon is significantly shorter than in red cones (*post-hoc Tukey*: *crx:mYFP-2A-trβ2*, $p = 0\ .00644$; *gnat2:mYFP-2A-trβ2;mpv17*$^{-/-}$, $p = 0.\ 00883$, Fig. 12D). The lengths are not distinguishable from blue cone axons (*post-hoc Tukey*: *crx:mYFP-2A-trβ2*, $p = 0\ .\ 21190$; *gnat2:mYFP-2A-trβ2;mpv17*$^{-/-}$, $p = 0.\ 17500$, Fig. 12D) or UV cones axons (*post-hoc Tukey*: *crx:mYFP-2A-trβ2*, $p = 0\ .\ 10775$; *gnat2:mYFP-2A-trβ2;mpv17*$^{-/}$, $p = 0.\ 13379$, Fig. 12D).

On morphometrics, the mYFP-marked trβ2 gain-of-function cones have not become red cones, but nonetheless enhance red cone signal amplitudes. Gain-of-function trβ2 morphologically alters cones and appears to shift the metrics towards a larval blue-cone pattern.

Impact of excess thyroid hormone receptor β2 on development of zebrafish spectral signals

During zebrafish maturation, patterns of cone opsin mRNA expression change through interactions with a 'developmental factor' (Takechi and Kawamura, 2005). Green- and red- cone spectral peaks shift from shorter to longer wavelengths by adulthood (Nelson et al., 2019) as different members of gene-duplicated green (*Rh2*) and red (*lws*) opsin groups are sequentially expressed. In the present control data, the R2 opsin signal (Vu556) is largest in embryonic (5 dpf, 6dpf) and juvenile (12 dpf) ages but the R1 opsin signal (Vr575) attains equal amplitude status in adults, while, over the same developmental course, the UV cone signal (Vu358) diminishes (Fig. 13A, 13B, WT and *mpv17*$^{-/-}$ controls, gray bars). Introduction of gain-of-function trβ2 shifts native developmental patterns of opsin expression. In the adults of both *crx:trβ2* and *gnat2:trβ2* gain-of-function transgenics, UV- (Vu358), blue- (Vb415, Vb440) and green- (Vg460, Vg480, Vg500) cone signals are reduced or extinguished by adulthood. In embryos and juveniles mainly R2 signals (Vr556) are increased but in adults, R1 signals (Vr575) are increased (Fig. 13A, 13B). As early as 5 dpf the *crx:trβ2* transgene decreases UV- (Vu358) and B1- (Vb415) cone signals to 11% and 20% of WT control, significant reductions [UV, $t(2465) = 10.4$, $p = 5.8 \times 10^{-25}$; B1, $t(2465) = 5.74$, $p = 1.1 \times 10^{-8}$], while increasing R2-cone amplitude (Vr556) to 230% of control [$t(2465) = 9.5$, $p = 4.3 \times 10^{-21}$, Fig. 13A, 5dpf]. The altered pattern of signal amplitudes from cone types in *crx:trβ2* persists throughout development, with UV cone signals becoming undetectable from 6 dpf on through adulthood (Fig. 13A, 6dpf, 12 dpf, Adult) and there is a failure to detect blue and green cone signals after the 12-dpf juvenile stage (Fig. 13A, Adult). Signals from red cones increase throughout embryonic (5 dpf, 6 dpf), juvenile (12 dpf) and adult developmental stages. R2 cone amplitudes (Vr556) increase at both 5 dpf and 12 dpf [12 dpf: $t(1558) = 6.29$, $p = 3.9 \times 10^{-10}$] and R1 cone signals (Vr575) increase for 6-dpf embryos and for adults [6 dpf: $t(1825) = 2.72$, $p = 0.0067$; Adult: $t(2818) = 3.92$, $p = 9.2 \times 10^{-5}$; Fig. 13A].

The consequences of gain-of-function trβ2 expressed through the *gnat2* promoter are more gradual in developmental course (Fig. 13B). In the 5dpf *gnat2:mYFP-2A-trβ2* embryonic larvae, the overall distribution of signal amplitudes from cone types is not significantly different from those found in the control (*mpv17*$^{-/-}$) siblings. However, as in the *crx:trβ2* embryos, R2 cone signals (Vr556) trend larger [9%, $t(3091) = 3.39$, $p = 0.00070$]. Enhancement of R2 amplitudes progresses at later developmental times [6 dpf: 22%, $t(3422) = 9.42$, $p = 5.6 \times 10^{-23}$; 12 dpf: 50%, $t(2540) = 2.65$, $p = 0.0082$], but red-cone enhancement switches from R2 (Vr556) to R1 (Vr575) signals in adults, where the largest enhancement is seen [241%, $t(2953) = 4.86$, $p = 1.2 \times 10^{-6}$]. In adults the red-cone-signal increase becomes R1 selective, with no significant change seen in adult R2-cone amplitudes [$t(2953) = 1.52$, $p = 0.127$]. In *gnat2:trβ2*,

UV-cone signals (Vu358) persist through larval and juvenile stages, with amplitudes either not significantly different [5 dpf: $t(3091) = 0.563$, $p = 0.574$; 12 dpf: $t(2540) = 0.594$, $p = 0.553$] or less than control [6 dpf: 45%, $t(3422) = 5.36$, $p = 8.7 \times 10^{-8}$], but unlike the significant UV signals of adult controls [$t(1579) = 4.81$, $p = 1.7 \times 10^{-6}$], no UV-signal was detected in *gnat2:trβ2* adults (Fig. 13B). B1- and G1-cone signals persist in *gnat2:trβ2* adults but are significantly reduced in amplitude as compared to controls [B1: 37%, $t(2953) = 2.97$, $p = 0.0030$; G1, 50%, $t(2953) = 2.23$, $p = 0.024$].

Discussion

Modeling of cone signals from zebrafish retinas yielded estimates of signal contributions from 8 spectrally distinct cone types during embryonic, juvenile, and adult developmental stages. When applied to trβ2 gain-of-function transgenics, the technique provided a window on the actions of this red-cone transcription factor in the differentiation and development of electrical signals from these cone types and others, a downstream manifestation of genetic impact. Two transgenics were studied. In *crx:mYFP-2A-trβ2*, the *crx* promoter introduced trβ2 into the cytoplasm of most retinal progenitor cells, whether ultimately fated to become cone cells or not (Shen and Raymond, 2004). In *gnat2:mYFP-2A-trβ2*;*mpv17*$^{-/-}$, the *gnat2* promoter added trβ2 to all differentiated cone types, including those to which it is not native, as well as adding an extra dose to the red-opsin cones where it is normally expressed (Ng et al., 2001; Suzuki et al., 2013). Only minor alterations in the amplitudes or kinetics of cone signals, as isolated from ERG signals by blockade of the cone synapse, were seen for step functions of light. In *crx:mYFP-2A-trβ2* larvae, response amplitudes were larger than WT controls, as was the spread of amplitudes. In the adults, peak times of both onset and offset waveform elements were significantly faster. Neither alteration suggested a major influence on phototransduction. In *gnat2:mYFP-2A-trβ2*;*mpv17*$^{-/-}$ there were no significant changes either in amplitudes or in onset and offset kinetics. But significant changes were found for both gain-of-function transgenics in the relative contributions from different cone types in response to spectral stimulation of retinas.

The trβ2 transcription factor is essential for red-cone development. Red-cone opsin immunoreactivity was absent in zebrafish *trβ2*$^{-/-}$ mutants of all ages, and in these mutants, long-wavelength stimuli did not evoke either ERG cone signals or activate behavioral responses (Deveau et al., 2020). In red-cone development the thyroid hormone receptor β2 affects multiple genetic targets. A first target is *trβ2* gene expression itself. Thyroid hormone receptor β2 is required to promote its own expression. In the transgenic-mutant zebrafish *trβ2* $^{-/-}$*;trβ2:tdTomato*, no fluorescence was expressed by the trβ2 reporter gene (Deveau et al., 2020), implying that the trβ2 transcription factor is a required *trβ2* promotor. This positive feedback loop of trβ2 acting as its own transcription factor may be like a switch which can be flipped ON permanently, creating a red cone. In retinal progenitors, the introduction of trβ2 by the *crx:trβ2* gain-of-function transgene flips this switch ON, activating a second trβ2 downstream target, promotion of *lws1* and *lws2* opsin genes, and expression of LWS opsins. Activation of the 'red-cone' genetic program early in development by the *crx:trβ2* transgene leads to overproduction of red-opsin immunoreactive cones, and greater amplitude red-cone spectral signals in embryos, juveniles, and adults. Nonetheless not all retinal progenitors become red cones, as seen by a select group of embryonic retinal bipolar cells that also mark for the *crx:trβ2* transgene. The *gnat2:trβ2* gain-of-function transgene also increases the embryonic density of red-opsin immunoreactive cones, but many of these are mixed-opsin types. In a developmentally delayed action, *gnat2:trβ2* increases the signal amplitudes of red cones, but this enhancement, while ultimately comparable in size to *crx:trβ2*, is slower to develop, fully evident in adulthood but only barely evident in 5-dpf embryos.

A third action of trβ2 is suppression of UV-cones. Transgene reporters for *trβ2* gene activity are not active in differentiated zebrafish UV cones (Suzuki et al., 2013). In mouse, deletion of *trβ2* caused an increase in S-opsin immunoreactive cones (Ng et al., 2001). In zebrafish, amplitudes of UV-cone signals increased in both adult and embryonic *trβ2* mutants and in embryonic heterozygous mutants (Deveau et al., 2020). These observations are consistent with a suppressive effect of native trβ2 on UV-cone development and maintenance. Both mouse S-cones and zebrafish UV cones belong to the UV-opsin molecular phylogenetic group (Terakita, 2005). With the progression of developmental stages in teleosts, the role of UV cones typically diminishes (Cheng et al., 2006; Carleton, 2009; Nelson et al., 2019).

Here we show that zebrafish gain-of-function transgenes provide further confirmation of the suppressive action of trβ2 on UV-cone development and maintenance. With progenitor-cell expression of trβ2 in gain-of-function *crx:trβ2* embryos, UV-opsin immunoreactive cones are greatly reduced in number, and UV-cone signals are not detected after embryonic day 5. UV-cone signals are also suppressed in gain-of-function *gnat2:trβ2* zebrafish, but with more delay. Such signals are not eliminated until adulthood, and UV-opsin immunoreactivity is still abundant in embryos and juveniles. The *gnat2:trβ2* transgene introduces exogenous trβ2 only into differentiated cone cells but targets all spectral types including the UV cones. In embryos and juveniles red-cone opsin immunoreactivity is induced within UV cones, creating mixed opsin immunoreactive cones in addition to the native solely UV-opsin immunoreactive cones. A reporter transgene suggests that in mixed-opsin UV cones, activity of the UV-opsin gene (*sws1*) is blocked by the gain-of-function trβ2 and the mixed-opsin UV cone is no longer able to synthesize UV opsin (SWS1). This may be a path by which UV cones are gradually lost, and/or converted to red cones.

In a fourth action, we found that overproduction of trβ2 in zebrafish gain-of-function transgenics reduced or eliminated green-cone and blue-cone signals. The Vb415 (B1) and Vg460 (G1) signals were significant in *crx:trβ2* embryos and juveniles but lost in adults. G1-cone signals might be either increased or decreased compared to controls in *gnat2:trβ2* embryos but both were reduced in adults, while in adult zebrafish *trβ2*$^{-/-}$ mutants (Deveau et al., 2020) green-cone signals increased significantly in amplitude. These observations suggest a late-stage inhibitory effect on green cones. Knockout of the zebrafish homeobox transcription factor *six7* eliminates green-cone Rh2 mRNAs in adults and *six*6 knockouts adversely affect blue-cone SWS2 mRNA (Ogawa et al., 2015; Ogawa et al., 2019). An association of these factors with blue and green cones was made by single-cell sequencing and machine learning methods (Ogawa and Corbo, 2021). Perhaps there is an inhibitory action of trβ2 on these homeobox genes.

A fifth action of trβ2 is influencing the spectral balance of the two zebrafish gene duplicated red opsins (LWS1, LWS2). Individual zebrafish red cones express either one or the other of these opsin genes but not both (Tsujimura et al., 2010; Mackin et al., 2019). In situ hybridization indicates that red cones in embryonic and larval zebrafish choose mainly the *lws2* opsin gene, while adult red cones are more likely to transcribe *lws1*, particularly in peripheral retina (Takechi and Kawamura, 2005). The present analysis of cone PIII spectral data, both for WT and *mpv17*$^{-/-}$ controls, support this molecular developmental profile. LWS2 (R2) opsin signals were the largest, and most often the only, red-cone signals detected in embryos and juveniles of control animals, but about equal amplitudes of both R1 and R2 signals appeared in adult controls. In gain-of-function trβ2 larvae and juveniles, with one exception, it was R2 signals that increased. In adults, it was R1 signals that increased and became the largest-amplitude cone spectral signal, shifting retinal spectral peaks from mid-spectrum in controls to long wavelengths in trβ2 gain-of-function transgenics. There is a possibly related augmentation of LWS1 mRNA in adult *six7* transcription

factor knockouts (Ogawa et al., 2015), suggesting that this transcription factor inhibits LWS1, but might itself be inhibited by trβ2.

The *lws1* and *lws2* genes are duplications arranged in tail-to-head manner on chromosome 11 under the control of an upstream LWS-activating region. It appears that *lws1* expression is under developmental control by a 2.6 kb upstream region, but that *lws2* is constitutively active, unless *lws1* is activated (Tsujimura et al., 2010). Present results suggest that trβ2 promotes the activation of *lws1* through developmental factors. However in larvae, *lws1* can be activated by thyroid hormone treatment (Mackin et al., 2019). It is unclear whether this is caused by a second pathway, or by an even greater activation by the bound state of trβ2 than achieved by extra, gain-of function, unbound trβ2.

A sixth action of trβ2 is the exercise of control over cone morphology. Larval cone morphologies in both the studied gain-of-function transgenics were abnormal. In *gnat2:trβ2*, where the transgene was expressed in all cone types, cones expressing the fluorescent transgene reporter did not look like red cones, resembled none of the control cone-type morphologies, but had a transgenic shape closest in morphometrics to, but by no means fully resembling, the control larval blue cones. There appears to be an early alteration of the native morphologies by the gain-of-function trβ2. The genetic basis is not known. Clearly trβ2 is importantly involved in large swaths of cone development, including the formation of adult double cones, with characteristic Arrestin 3a antigenicity (Deveau et al., 2020). Thyroid hormone receptor β2 pathways are not yet fully elaborated, but studies of zebrafish mutants and gain-of function transgenics expand the inventory of genetic and physiological targets and provide a role in development.

References

Allison WT, Barthel LK, Skebo KM, Takechi M, Kawamura S, Raymond PA (2010) Ontogeny of cone photoreceptor mosaics in zebrafish. Journal of Comparative Neurology 518:4182-4195.

Applebury M, Antoch M, Baxter L, Chun L, Falk J, Farhangfar F, Kage K, Krzystolik M, Lyass L, Robbins J (2000) The murine cone photoreceptor: a single cone type expresses both S and M opsins with retinal spatial patterning. Neuron 27:513-523.

Baylor D, Fuortes M (1970) Electrical responses of single cones in the retina of the turtle. The Journal of Physiology 207:77-92.

Bian W-P, Pu S-Y, Xie S-L, Wang C, Deng S, Strauss PR, Pei D-S (2021) Loss of mpv17 affected early embryonic development via mitochondria dysfunction in zebrafish. Cell death discovery 7:1-10.

Brockerhoff SE, Rieke F, Matthews HR, Taylor MR, Kennedy B, Ankoudinova I, Niemi GA, Tucker CL, Xiao M, Cilluffo MC, Fain GL, Hurley JB (2003) Light stimulates a transducin-independent increase of cytoplasmic Ca2+ and suppression of current in cones from the zebrafish mutant nof. J Neurosci 23:470-480.

Carleton K (2009) Cichlid fish visual systems: mechanisms of spectral tuning. Integrative zoology 4:75-86.

Cheng CL, Flamarique IN, Hárosi FI, Rickers - Haunerland J, Haunerland NH (2006) Photoreceptor layer of salmonid fishes: transformation and loss of single cones in juvenile fish. Journal of Comparative Neurology 495:213-235.

Chinen A, Hamaoka T, Yamada Y, Kawamura S (2003) Gene duplication and spectral diversification of cone visual pigments of zebrafish. Genetics 163:663-675.

Connaughton VP, Nelson R (2000) Axonal stratification patterns and glutamate-gated conductance mechanisms in zebrafish retinal bipolar cells. J Physiol 524:135-146.

Connaughton VP, Nelson R (2021) Ganglion cells in larval zebrafish retina integrate inputs from multiple cone types. Journal of Neurophysiology 126:1440-1454.

D'Agati G, Beltre R, Sessa A, Burger A, Zhou Y, Mosimann C, White RM (2017) A defect in the mitochondrial protein Mpv17 underlies the transparent casper zebrafish. Developmental Biology 430:11-17.

Dartnall H, JA (1953) The interpretation of spectral sensitivity curves. British Medical Bulletin 9:24-30.

Deveau C, Jiao X, Suzuki SC, Krishnakumar A, Yoshimatsu T, Hejtmancik JF, Nelson RF (2020) Thyroid hormone receptor beta mutations alter photoreceptor development and function in Danio rerio (zebrafish). PLoS genetics 16:e1008869.

Engstrom K (1960) Cone types and cone arrangement in the retina of some cyprinids. . Acta Zoologica 41:277-295.

Grant GB, Dowling JE (1995) A glutamate-activated chloride current in cone-driven ON bipolar cells of the white perch retina. J Neurosci 15:3852-3862.

Grant GB, Dowling JE (1996) On bipolar cell responses in the teleost retina are generated by two distinct mechanisms. J Neurophysiol 76:3842-3849.

Hughes A, Saszik S, Bilotta J, Demarco PJ, Jr., Patterson WF, 2nd (1998) Cone contributions to the photopic spectral sensitivity of the zebrafish ERG. Visual Neuroscience 15:1029-1037.

Jacobs GH, Neitz J, Deegan II JF (1991) Retinal receptors in rodents maximally sensitive to ultraviolet light. Nature 353:655.

Kennedy BN, Alvarez Y, Brockerhoff SE, Stearns GW, Sapetto-Rebow B, Taylor MR, Hurley JB (2007) Identification of a Zebrafish Cone Photoreceptor-Specific Promoter and Genetic Rescue of Achromatopsia in the nof Mutant. Invest Ophthalmol Vis Sci 48:522-529.

Mackin RD, Frey RA, Gutierrez C, Farre AA, Kawamura S, Mitchell DM, Stenkamp DL (2019) Endocrine regulation of multichromatic color vision. Proceedings of the National Academy of Sciences 116:16882-16891.

Marks W (1965) Visual pigments of single goldfish cones. The Journal of Physiology 178:14.

Nelson RF, Singla N (2009) A spectral model for signal elements isolated from zebrafish photopic electroretinogram. Visual Neuroscience 26:349-363.

Nelson RF, Balraj A, Suresh T, Torvund MM, Patterson SS (2019) Strain variations in opsin peaks in situ during zebrafish development. Visual neuroscience 36:E010.

Ng L, Hurley JB, Dierks B, Srinivas M, Saltó C, Vennström B, Reh TA, Forrest D (2001) A thyroid hormone receptor that is required for the development of green cone photoreceptors. Nature genetics 27:94-98.

Ogawa Y, Corbo JC (2021) Partitioning of gene expression among zebrafish photoreceptor subtypes. Scientific reports 11:1-13.

Ogawa Y, Shiraki T, Kojima D, Fukada Y (2015) Homeobox transcription factor Six7 governs expression of green opsin genes in zebrafish. Proc R Soc B 282:20150659.

Ogawa Y, Shiraki T, Asano Y, Muto A, Kawakami K, Suzuki Y, Kojima D, Fukada Y (2019) Six6 and Six7 coordinately regulate expression of middle-wavelength opsins in zebrafish. Proceedings of the National Academy of Sciences 116:4651-4660.

Palacios AG, Goldsmith TH, Bernard GD (1996) Sensitivity of cones from a cyprinid fish (Danio aequipinnatus) to ultraviolet and visible light. Visual Neuroscience 13:411-421.

Raymond PA, Barthel LK, Rounsifer ME, Sullivan SA, Knight JK (1993) Expression of rod and cone visual pigments in goldfish and zebrafish: a rhodopsin-like gene is expressed in cones. Neuron 10:1161-1174.

Shen Y-c, Raymond PA (2004) Zebrafish cone-rod (crx) homeobox gene promotes retinogenesis. Developmental biology 269:237-251.

Sillman AJ, Ito H, Tomita T (1969) Studies on the mass receptor potential of the isolated frog retina: I. General properties of the response. Vision Research 9:1435-1442.

Suzuki SC, Bleckert A, Williams PR, Takechi M, Kawamura S, Wong RO (2013) Cone photoreceptor types in zebrafish are generated by symmetric terminal divisions of dedicated precursors. Proceedings of the National Academy of Sciences of the United States of America 110:15109-15114.

Takechi M, Kawamura S (2005) Temporal and spatial changes in the expression pattern of multiple red and green subtype opsin genes during zebrafish development. Journal of Experimental Biology 208:1337-1345.

Takechi M, Hamaoka T, Kawamura S (2003) Fluorescence visualization of ultraviolet-sensitive cone photoreceptor development in living zebrafish. FEBS Letters 553:90-94.

Takechi M, Seno S, Kawamura S (2008) Identification of cis-Acting Elements Repressing Blue Opsin Expression in Zebrafish UV Cones and Pineal Cells. Journal of Biological Chemistry 283:31625-31632.

Terakita A (2005) The opsins. Genome biology 6:213.

Tsujimura T, Hosoya T, Kawamura S (2010) A single enhancer regulating the differential expression of duplicated red-sensitive opsin genes in zebrafish. PLoS genetics 6:e1001245.

Weiss AH, Kelly JP, Bisset D, Deeb SS (2012) Reduced L-and M-and increased S-cone functions in an infant with thyroid hormone resistance due to mutations in the THRβ2 gene. Ophthalmic genetics 33:187-195.

Wong KY, Gray J, Hayward CJ, Adolph AR, Dowling JE (2004) Glutamatergic mechanisms in the outer retina of larval zebrafish: analysis of electroretinogram b- and d-waves using a novel preparation. Zebrafish 1:121-131.

Yin J, Brocher J, Linder B, Hirmer A, Sundaramurthi H, Fischer U, Winkler C (2012) The 1D4 antibody labels outer segments of long double cone but not rod photoreceptors in zebrafish. Investigative ophthalmology & visual science 53:4943-4951.

Yoshimatsu T, Williams PR, D'Orazi FD, Suzuki SC, Fadool JM, Allison WT, Raymond PA, Wong RO (2014) Transmission from the dominant input shapes the stereotypic ratio of photoreceptor inputs onto horizontal cells. Nature communications 5.

Figure Legends

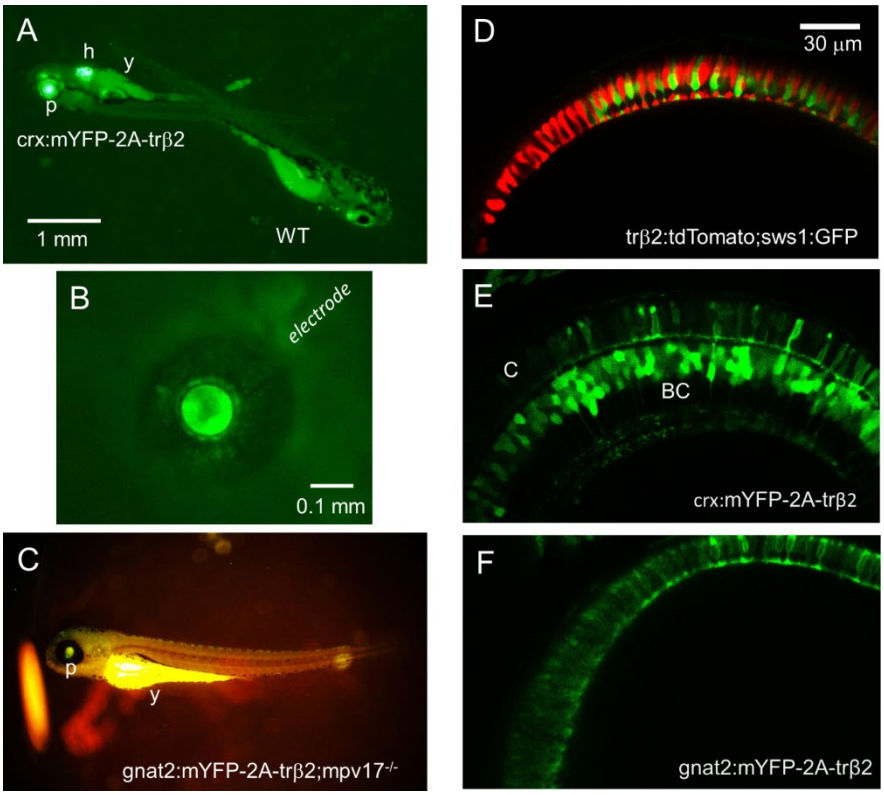

Figure 1. Transgene reporter fluorescence of *trβ2* gain-of-function larvae. ***A***, Larvae from outcrosses of *crx:mYFP-2A-trβ2* heterozygotes are either heterozygous or wild-type controls (WT). The heterozygotes are recognized by both pupil (p) and heart (h) fluorescence. The yolk sac (y) is autofluorescent. ***B***, The cornea of a transgenic eye isolated from a *crx:mYFP-2A-trβ2* larva is penetrated with a patch electrode for ERG recordings. The 5-day embryonic eye is less than 0.5 mm diameter. ***C***, The *gnat2:mYFP-2A-trβ2;mpv17*$^{-/-}$ gain-of-function phenotype is studied on a *roy orbison* (*mpv17*$^{-/-}$) control background. The darkly pigmented, non-reflective iris of this background strain aids in visualizing the dim transgenic fluorescence of the pupil (p). The yoke (y) is autofluorescent. (***D***, ***E***, ***F***) Live confocal imaging of retinas in 6 dpf larvae. ***D***, WT red (red) and UV (green) cone morphology visualized with *trβ2:tdTomato* and *sws1:GFP* fluorescent reporter transgenes. ***E***, The *mYFP* construct in the *crx:mYFP-2A-trβ2* transgene causes cones (C) and bipolar cells (BC) to fluoresce. ***F***, The *mYFP* construct in the transgene *gnat2:mYFP-2A-trβ2* marks only cone cells.

A

$$\textit{Equation 1.}\quad V = \sum_{i=1}^{8} Vm_i \times \frac{I}{I + \frac{k_i}{A(wlmax_i, wl)}}$$

B

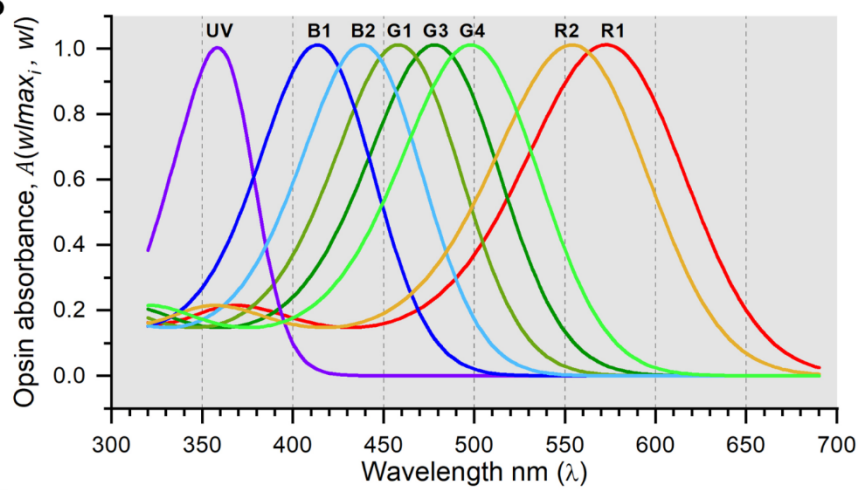

C

Cone index ('i', Eq. 1)	*Shorthand name*	*Common name*	*Opsin Gene*	*Peak wavelength (nm)*	*log of semi-saturation relative to UV*
1	UV	UV	*sws1*	358	0.0
2	B1	blue	*sws2*	415	0.0
3	B2	blue	unknown	440	0.5
4	G1	green	*RH2-1*	460	0.0
5	G3	green	*RH2-2* *RH2-3*	480	1.0
6	G4	green	*RH2-4*	500	1.0
7	R2	red	*lws2*	556	1.0
8	R1	red	*lws1*	575	1.0

Figure 2. Algorithm for weighting the signal strengths of the different cone types contributing to ERG spectral data. ***A***, Equation 1. Aspartate-isolated cone signals from zebrafish eyes are a summation of signals from 8 cone types, each distinguished by different maximal amplitudes (Vm_i), semi-saturation irradiances (k_i), and opsin peak absorbances ($wlmax_i$). There are 255 unique combinations of 8 opsins, each combination is a candidate to best model cone spectral responses in the ERG. ***B***, Spectral shapes of opsin absorbances [$A(wlmax_i, wl)$] are generated from 8th-order template polynomials (Palacios et al., 1996; Hughes et al., 1998) using Dartnall nomogram translations along the wavelength axis (Dartnall, 1953) to represent opsins of different peak wavelengths. ***C***, Parameters for each of the '*i*' cone types are numbered in order from short to long wavelengths. SWS, short-wavelength-sensitive opsins; RH2, rhodopsin-like green-cone opsins; LWS, long-wavelength-sensitive opsins.

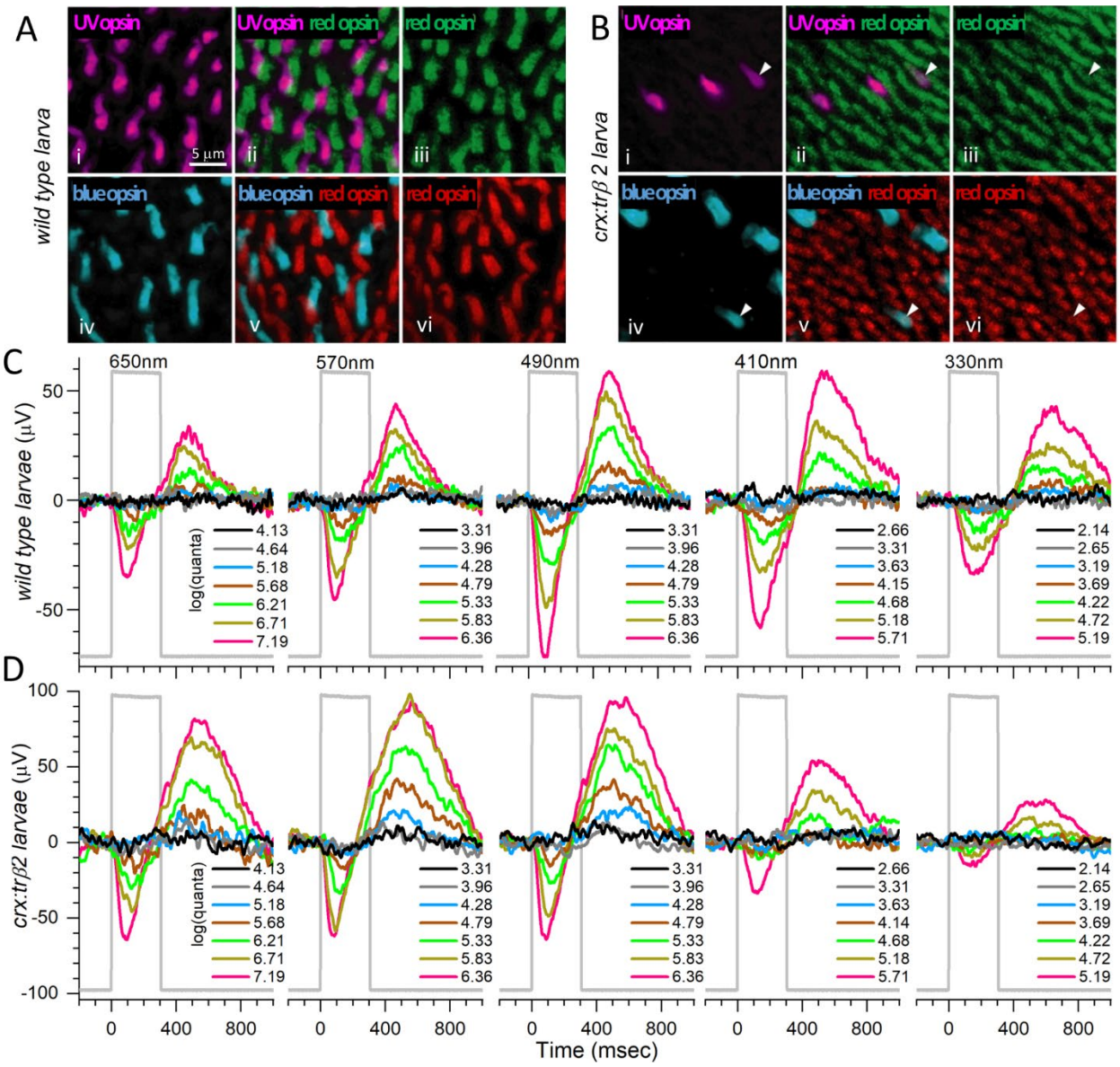

Figure 3. Cone distributions and spectral responses in larval embryonic WT and *crx:mYFP-2A-trβ2* retinas. ***Ai***, UV opsin (SWS1) immunoreactive cones in a WT retina. ***Aiii***, ***Avi***, Red opsin (LWS1, LWS2) immunoreactive cones in WT retinas. ***Aiv***, Blue opsin (SWS2) immunoreactive cones in a WT retina. ***Aii***, UV and red opsins are expressed in separate cones in a WT retina. ***Av***, Red- and blue-opsins are expressed in separate cones in a WT retina. ***Bi***, UV-opsin immunoreactive cones in a *crx:trβ2* retina. ***Biii***, ***Bvi***, Red opsin immunoreactive cones in *crx:trβ2* retinas. ***Biv***, Blue opsin immunoreactive cones in *crx:trβ2* retina. There are fewer UV and blue cones in *crx:trβ2* retinas than in WT retinas. ***Bii***, One *crx:trβ2* cone is immunoreactive for both UV and red opsins (arrowhead). ***Bv***, Arrowhead points to a *crx:trβ2* cone immunoreactive for both red and blue opsins. ***C***, Cone signals from a WT larval eye respond to all stimulus wavelengths yielding the largest amplitudes at 490 nm. ***D***, The larval *crx:trβ2* retina responds with maximal amplitudes at wavelengths 490, 570 and 650 nm but is less responsive than WT for 330 and 410 nm, wavelengths that stimulate blue and UV cones. ***A, B,*** 5-dpf larvae. ***C, D,*** 6-dpf larvae. Perfusion medium contains 20 mM Aspartate to isolate photoreceptor signals in the ERG. Five of the 9 stimulus-protocol wavelengths are illustrated. The stimulus irradiances [units of log(quanta·μm^{-2}·s^{-1})] appear to the right of stacked irradiance-response traces.

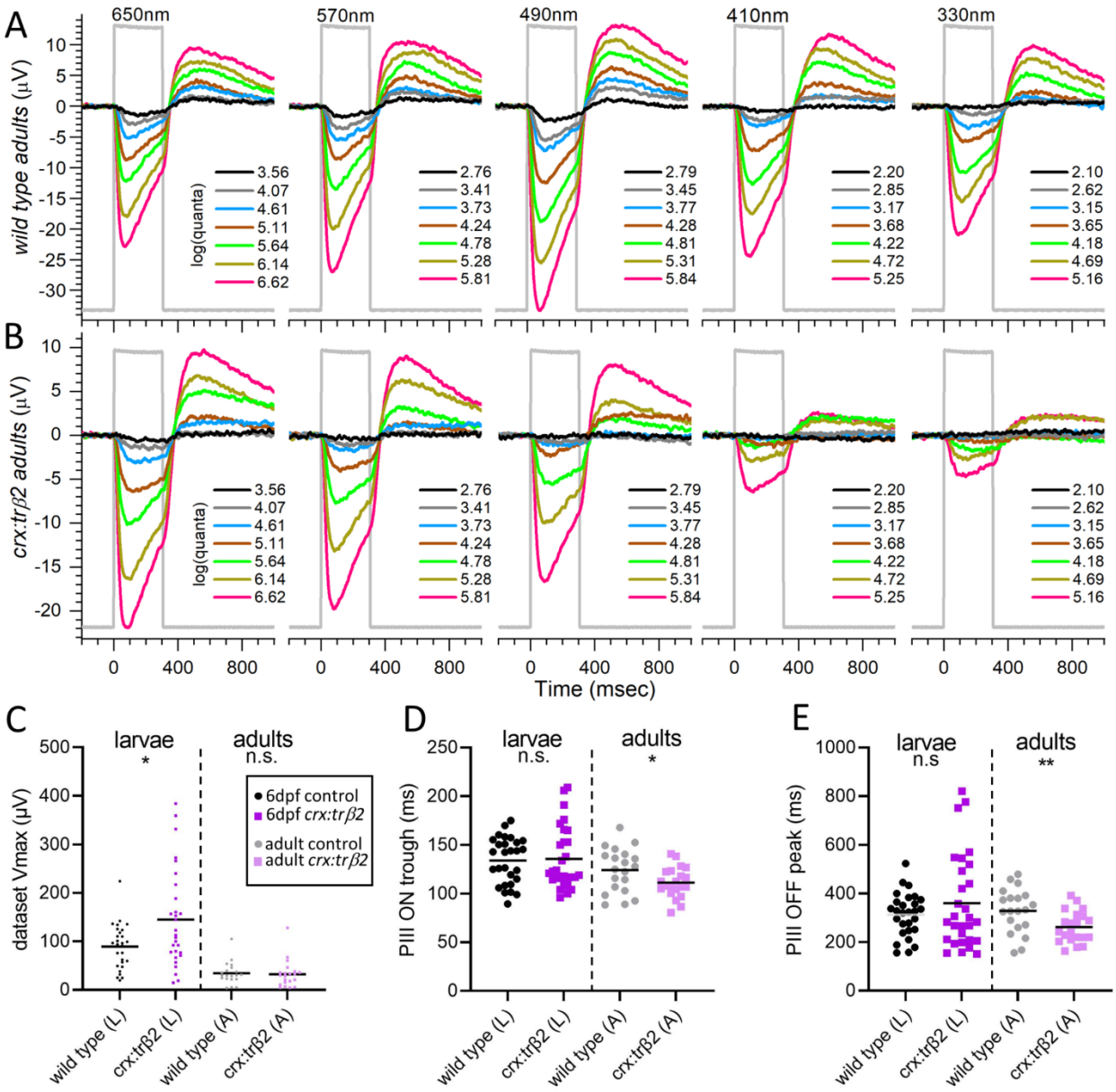

Figure 4. Cone spectral signals in WT and *crx:mYFP-2A-trβ2* adults. ***A***, In WT eyecups all wavelengths and almost all irradiances evoke signals, with a maximal response at 490 nm. ***B***, Cone signals from *crx:trβ2* eyecups are maximal at 650 nm. Responses to wavelengths that stimulate blue and UV cones (410 nm, 330 nm) are low in amplitude. In ***A***, and ***B***, adults are 8-18 mo. The perfusion medium contains 10 mM Aspartate to isolate cone signals. The nested responses are irradiance-response series at each wavelength, with irradiances given to the right of the traces in units of log(quanta·μm^{-2}·s^{-1}). ***C***, ***D***, ***E***, Properties of ERG cone-PIII waveforms in larval and adult, WT control and *crx:trβ2* retinas. ***C***, Distributions of maximal trough-to-peak amplitudes in larval and adult spectral datasets. ***D***, Cone-signal latency from stimulus onset to the minimum of the ON trough of cone signal are measured on the mean response of each 280-stimulus spectral dataset. ***E***, Cone-signal latency to the OFF peak in the mean responses of spectral datasets. OFF latencies are measured from stimulus offset. Asterisks (n.s., not significant) are probabilities that WT and *crx:trβ2* distributions differ in larvae or adults (Graphpad Prism convention, statistics given in text).

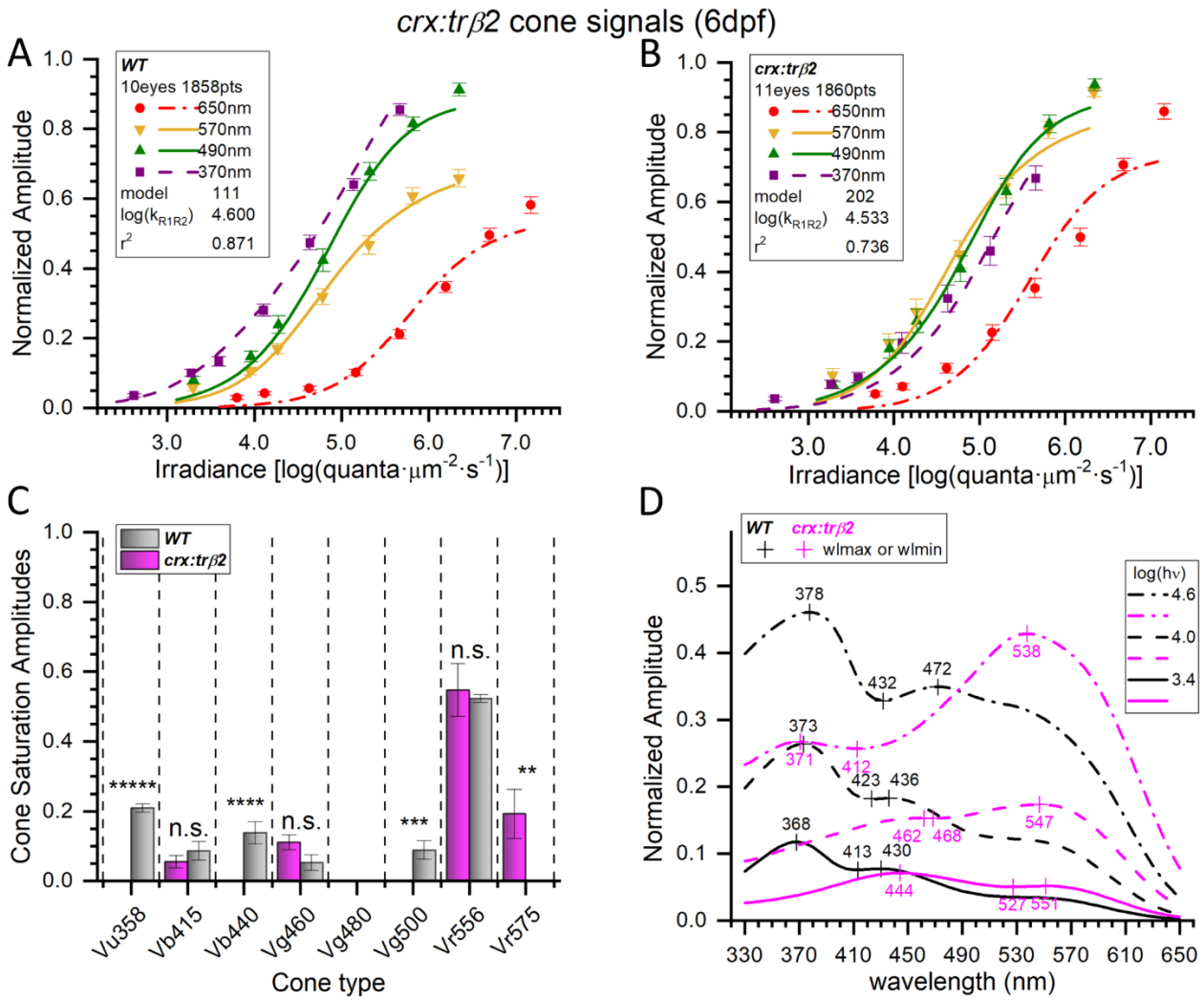

Figure 5. Spectral models of cumulative data from embryonic larval *crx:mYFP-2A-trβ2* and WT eyes. ***A***, Irradiance-response datapoints and model curves from WT eyes. Curves are generated by the optimal model (#111) as fit to 1858 spectral response amplitudes combined from 28 normalized datasets taken from 10 eyes (Fig. 1A, Eq. 1 algorithm). Response amplitudes are means ± SE of data extracted from the cumulative dataset. 370 nm, n = 23-28; 490-nm, n = 27-28; 570-nm; n = 23-28; 650-nm, n = 23-55. ***B***, Irradiance-response datapoints and optimal model curves from *crx:trβ2* eyes. The optimal model (#202) is fit to 1860 spectral points combined from 29 datasets taken from 11 eyes. Individual points: 370 nm, n = 22-28; 490 nm, n = 23-28; 570 nm, n = 27-28 points; 650 nm, n = 24-55. The *crx:trβ2* transgene moves curves and points along the irradiance axis as compared to WT. ***C***, In WT larval eyes, six cone types (gray bars) were detected by the optimal model. In *crx:trβ2* eyes, four cone signals were detected (magenta bars). Cone saturation amplitudes [Vm_i values (Eq. 1, Fig.2A) ± SE] are fractions of dataset maximal amplitudes. Asterisks denote significance of differences between WT and *crx:trβ2* (one or two sample t-tests; n.s., not significant; GraphPad Prism convention). Vu358 (UV, one sample test): $t(1822) = 17.8$, $p = 1.2 \times 10^{-65}$; Vb415 (B1): $t(3647) = 0.958$, $p = 0.338$; Vb440 (B2): $t(1822) = 4.27$, $p = 2.0 \times 10^{-5}$; Vg460 (G1): $t(3647) = 1.87$, $p = 0.062$; Vg500 (G4, one sample test): $t(1822) = 3.33$, $p = 8.8 \times 10^{-4}$; Vr556 (R2): $t(3647) = 0.318$, $p = 0.751$; Vr575 (R1): $t(1825) = 2.72$, $p = 0.0067$. ***D***, Spectral peaks shift to longer wavelengths for *crx:trβ2* (magenta) as compared to WT (black). Spectral curves are the modeled amplitudes that would be evoked by 3 different irradiances of constant quantal stimulation across the spectrum [3.4, 4.0, and 4.6 log(quanta·$\mu m^{-2}\cdot s^{-1}$)]. Spectral shapes differ with stimulus brightness. (***A***, ***B***) The log(k_{R1R2}) values are modeled R1-cone and R2-cone semi-saturation irradiances in log(quanta·$\mu m^{-2}\cdot s^{-1}$). (***A***, ***B***, ***C***, ***D***) 6-dpf larvae, 20 mM Aspartate medium.

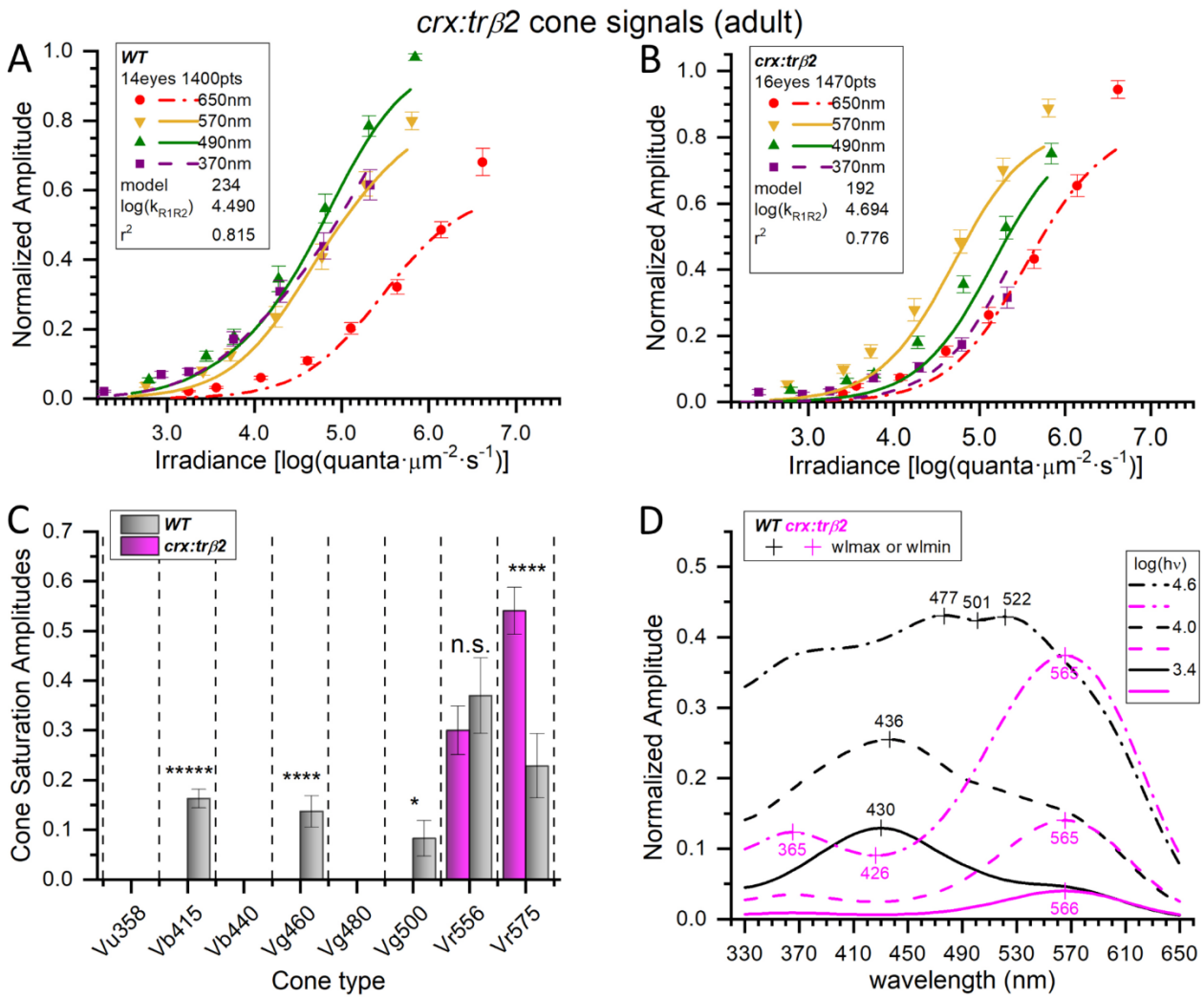

Figure 6. Adult *crx:mYFP-2A-trβ2* transgenics are red-cone dichromats. ***A***, WT cone-PIII irradiance-response curves and datapoints at four stimulus wavelengths. The 370-, 490- and 570-nm amplitudes are means (± SE) from the cumulative dataset (n = 20 except 650-nm, n = 20 or 40). Curves are generated from the optimal model (#234) fit to a cumulative 1400 responses at 7 irradiances for each of 9 wavelengths as compiled from 20 spectral datasets acquired in 14 WT adult eyecups. ***B***, The *crx:trβ2* gain-of-function transgene moves irradiance-response points and model curves along the irradiance axis as compared to WT. The model generating the curves (#192) is fit to 1470 cumulative responses compiled from 21 datasets acquired from 16 *crx:trβ2* eyecups. The amplitudes (± SE) are means (370-, 490-, and 570- nm, n = 21; 650 nm, n = 21 or 42). ***C***, Signals from five blue, green, or red cone types were detected in WT adult eyecups (gray bars) but signals from only the two red-cone types were detected in *crx:trβ2* eyecups (magenta bars). Fit values of cone saturation amplitudes (Vm_i, Eq. 1, Fig. 2A) are plotted on a dataset-normalized scale (± SE). Significant differences in amplitudes of cone types between WT and *crx:trβ2* are denoted by asterisks (GraphPad Prism convention, n.s., not significant). Vb415 (B1, one sample test): $t(1373) = 8.77$, $p = 5.4 \times 10^{-18}$; Vg460 (G1, one sample test): $t(1373) = 4.36$, $p = 1.4 \times 10^{-5}$; Vg500 (G3, one sample test): $t(1373) = 2.30$, $p = 0.021$; Vr556(R2): $t(2818) = 0.782$, $p = 0.434$; Vr575 (R1): $t(2818) = 3.91$, $p = 9.2 \times 10^{-5}$. ***D***, Model spectral curves for adult WT (black) and *crx:trβ2* (magenta) eyecups. The *crx:trβ2* transgene shifts sensitivity peaks to long wavelengths at all stimulus irradiances. Curves are modeled for constant quantal stimuli at 3.4, 4.0, and 4.6 log(quanta·$\mu m^{-2}\cdot s^{-1}$). (***A***, ***B***) The log(k_{R1R2}) values are the irradiance semi-saturation values in log(quanta·$\mu m^{-2}\cdot s^{-1}$) for both R1 and R2 cones. (***A***, ***B***, ***C***, ***D***). 8-18-month adults, 10 mM Aspartate medium.

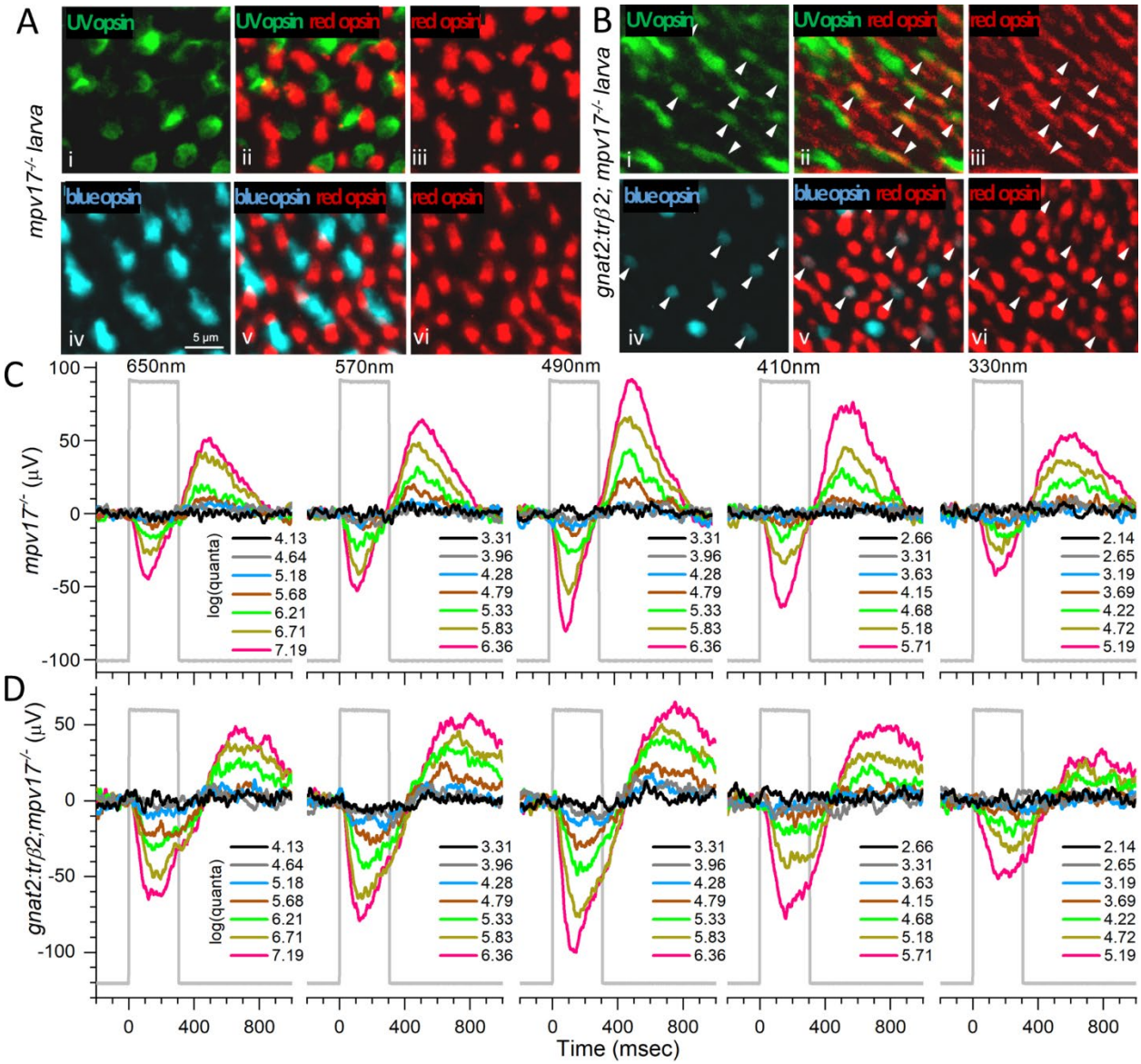

Figure 7. Larval cone distributions and spectral responses in *gnat2:mYFP-2A-trβ2;mpv17*$^{-/-}$ eyes and controls. ***Ai***, UV opsin (SWS1) opsin immunoreactive cones in control (*roy orbison mpv17*$^{-/-}$) retinas. ***Aiv***, Blue opsin (SWS2) immunoreactive cones in control retina. ***Aiii***, ***Avi***, Red (LWS1, LWS2) opsin immunoreactive cones in control retina. ***Aii***, UV and red opsins are expressed in separate cones in control retina. ***Av***, Blue and red opsins are expressed in separate cones in control retina. ***Bi***, UV opsin immunoreactive cones in *gnat2:trβ2* retina. ***Biv***, Blue opsin immunoreactive cones in *gnat2:trβ2* retina. ***Biii***, ***Bvi***, Red opsin immunoreactive cones in *gnat2:trβ2* retinas. ***Bii***, ***Bv***, Red opsins are often expressed in the blue or UV opsin immunoreactive cones of *gnat2:trβ2* retinas (arrowheads, ***Bii***, ***Bv***). ***A***, ***B***, 12-dpf larvae. ***C***, ***D***, 6-dpf larvae. Cone signals in *mpv17*$^{-/-}$ control and *gnat2:trβ2* retinas are robust at all wavelengths with greatest amplitudes at 490 nm. The perfusion medium contains 20 mM Aspartate to isolate cone signals. Stimulus irradiances [log(quanta·μm^{-2}·s^{-1})] appear in the legends to the right of irradiance-response trace stacks.

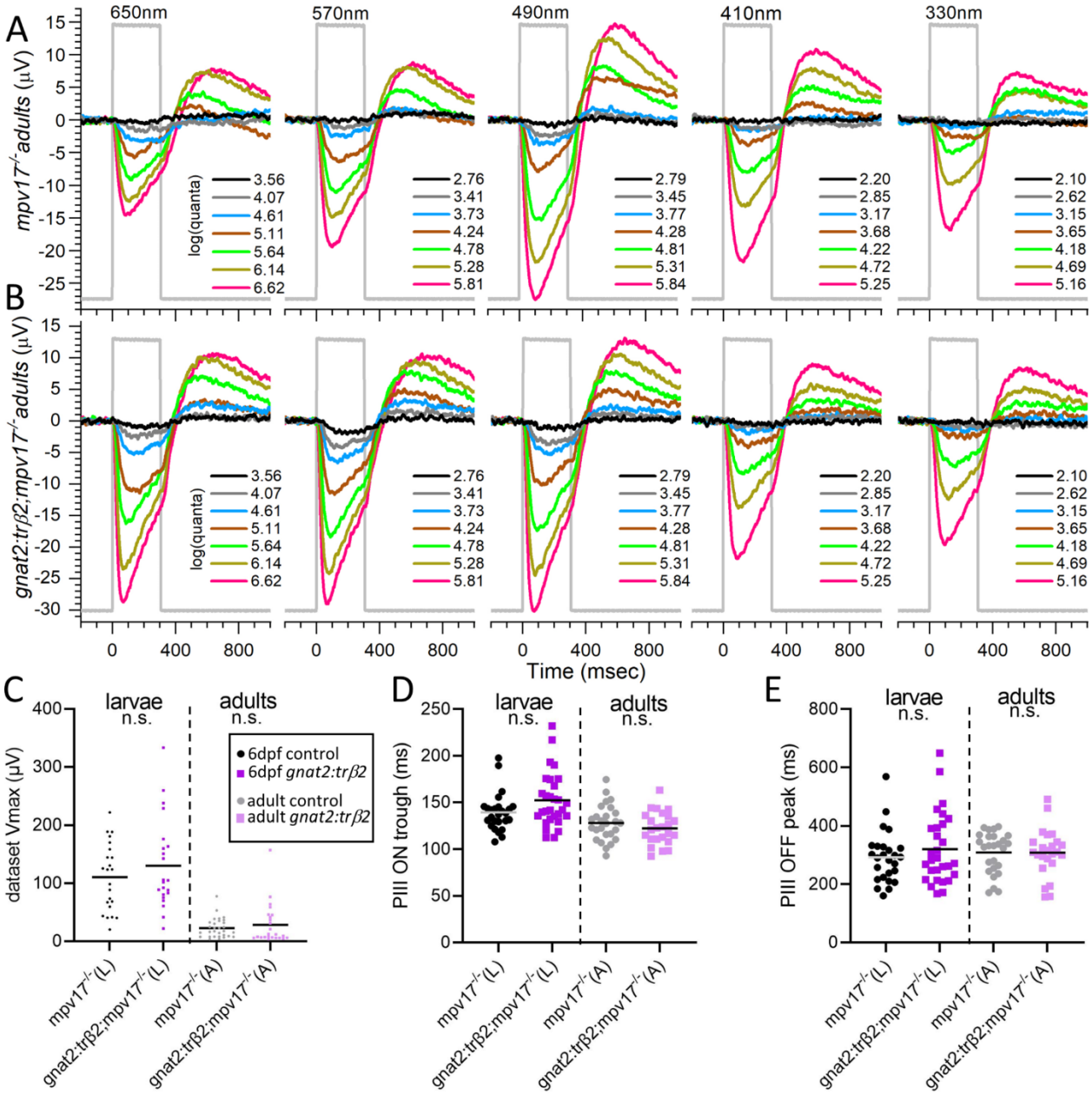

Figure 8. Cone PIII spectral properties in control and *gnat2:mYFP-2A-trβ2;mpv17*$^{-/-}$ adults. ***A***, Cone signals in an *mpv17*$^{-/-}$ control eyecup are evoked by all stimulus wavelengths and all but the dimmest irradiances (black). The largest amplitudes occur at 490 nm. ***B***, Cone signals from a *gnat2:trβ2* eyecup are stimulated by all wavelengths and irradiances. Greatest amplitudes occur at 650, 570, and 490 nm. ***A***, ***B***, Adults are 8-18 mo. Eyecups are perfused with medium containing 10 mM Aspartate to isolate retinal cone signals. Stimulus irradiances [log(quanta·µm^{-2}·s^{-1})] appear in the legends to the right of irradiance-response waveform stacks. ***C***, Voltage distributions of maximal trough-to-peak amplitudes found in spectral datasets. ***D***, Cone-signal latencies from stimulus onset to the minimum in the ON trough. ***E***, Cone-signal latency from stimulus offset to the OFF peak. ***C***, ***D***, ***E***, The 'n.s.' labels on all distributions indicate that that *mpv17*$^{-/-}$ controls did not significantly differ from *gnat2:trβ2* transgenics in waveform characteristics (*p*-values given in text). Peak amplitudes (Vmax), trough (PIII ON trough) and peak (PIII OFF peak) latencies are measured on the mean waveforms from each 70-stimulus spectral dataset.

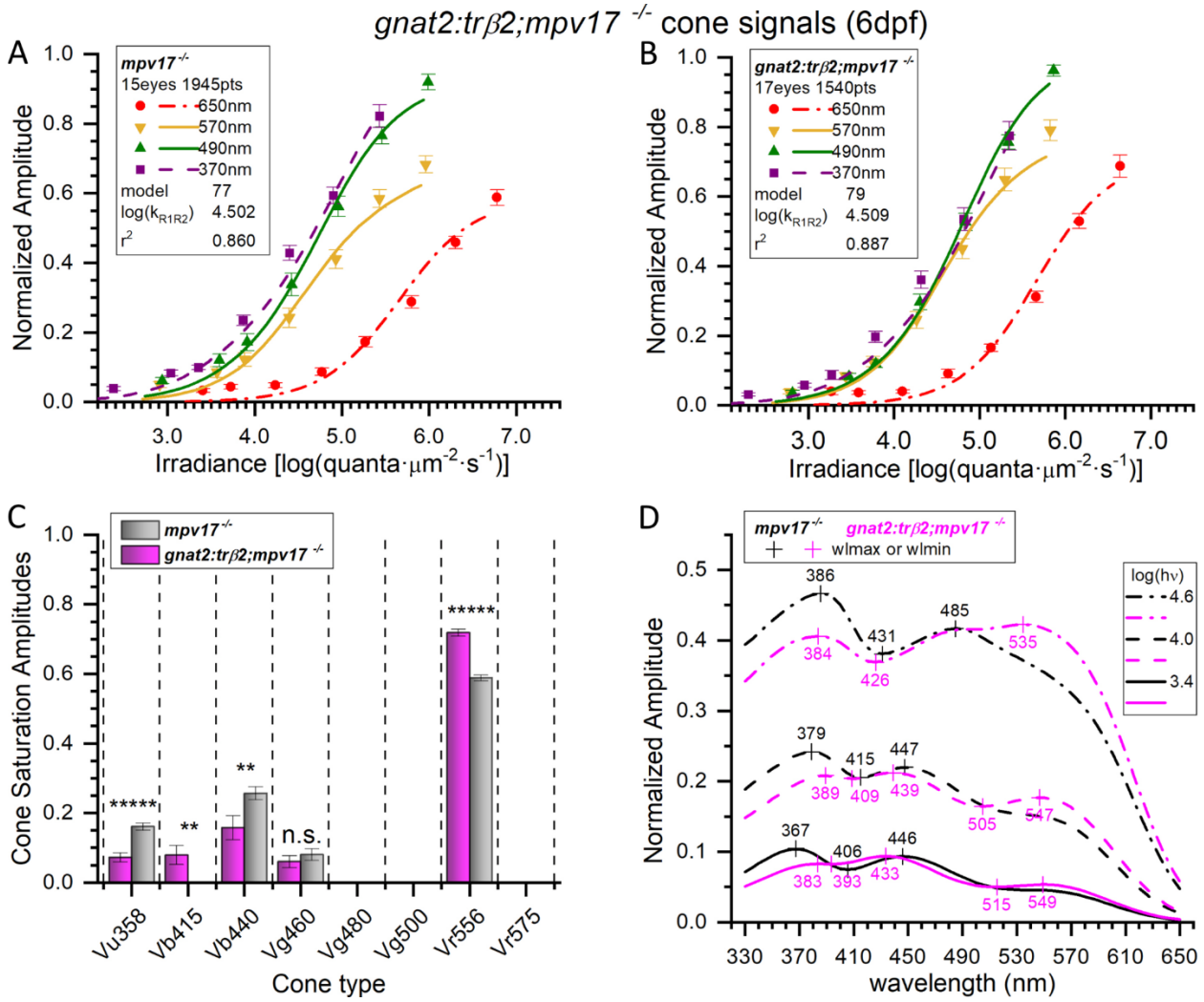

Figure 9. Spectral properties of embryonic cone signals from *gnat2:mYFP-2A-trβ2;mpv17*$^{-/-}$ larval eyes and *mpv17*$^{-/-}$ controls. ***A***, Control (*mpv17*$^{-/-}$) irradiance-response points and optimal model curves. The model (#77) was fit to 1945 spectral response amplitudes, combined from 28 datasets taken from 15 eyes. The points are subsets of the cumulative data. The 370-, 490- and 570-nm amplitudes are means (± SE), n = 27 or 28; 650-nm means, n = 28 or 56. ***B***, The *gnat2:trβ2* irradiance-response points and model curves. The gain-of-function trβ2 induces more bunching of the 370 nm, 490 nm, and 570 nm irradiance-response functions than seen in controls. The model (#79) was fit to 1540 spectral points, combined from 22 datasets taken from 17 eyes. The 370-nm, 490-nm, and 570-nm amplitudes are means (± SE), n = 22; 650-nm, n = 22 or 44. ***C***, Four cone types were detected in cone-signals isolated from *mpv17*$^{-/-}$ control eyes (gray bars) but five types proved significant in *gnat2:trβ2* eyes (magenta bars). Cone saturation amplitudes (Vm_i, Eq. 1, Fig. 2A) are fractions of maximal dataset amplitudes (± SE). Asterisks represent the significance of amplitude differences between *mpv17*$^{-/-}$ control and *gnat2:trβ2* (GraphPad Prism convention, n.s., not significant). Vu358 (UV): $t(3422) = 5.37$, $p = 8.7 \times 10^{-8}$; Vb415 (B1, one sample test): $t(1511) = 2.90$, $p = 0.0038$; Vb440 (B2): $t(3422) = 2.62$, $p = 0.0081$; Vg460 (G1): $t(3422) = 0.851$, $p = 0.395$; Vr556 (R2): $t(3422) = 9.94$, $p = 5.6 \times 10^{-23}$. ***D***, Model spectral curves for *mpv17*$^{-/-}$ controls and *gnat2:trβ2* larval eyes for constant quantal irradiances of 3.4, 4.0, and 4.6 log(quanta·μm^{-2}·s^{-1}). There is greater long-wavelength sensitivity, and lesser short-wavelength sensitivity in the trβ2 gain-of-function transgenic. ***A***, ***B***, The log(k_{R1R2}) values are the modeled R1- or R2- cone semi-saturation irradiances in log(quanta·μm^{-2}·s^{-1}). ***A***, ***B***, ***C***, ***D***, 6-dpf larvae, 10 mM Aspartate medium.

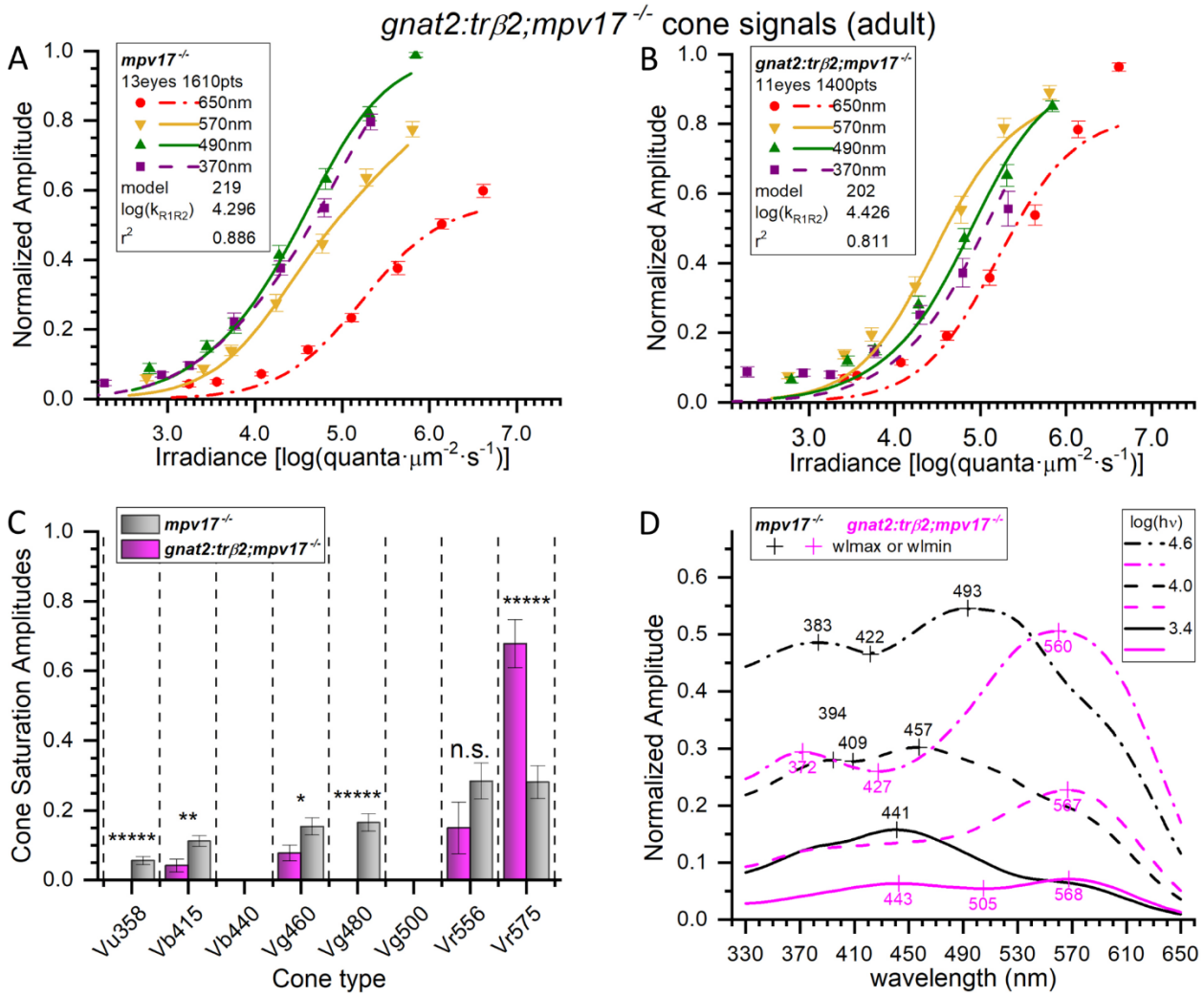

Figure 10. Spectral signals from cone types in adult *gnat2:mYFP-2A-trβ2* transgenics and *mpv17*$^{-/-}$ controls. ***A***, Control (*mpv17*$^{-/-}$) irradiance-response amplitudes and model curves at four wavelengths. The optimal model (#219) was fit to 1610 responses (all wavelengths) combined from 23 datasets taken from 13 eyecups. The 370-nm, 490-nm and 570-nm amplitudes are means (± SE), *n* = 23; 650-nm, *n* = 23 or 46. ***B***, Irradiance-response amplitudes and model curves for *gnat2:trβ2*. The transgene shifts 370-nm and 490-nm irradiance-response functions from the left of the 570-nm curve (control) to the right of the 570-nm curve (transgenic). The spectral algorithm was fit to 1400 points combined from 20 datasets accumulated from 11 eyecups. The 370-nm, 490-nm, and 570-nm amplitudes are means (± SE), *n* = 23; 650-nm, *n* = 23 or 46. ***C***, In adults, significant signals from six cone types were detected in the cone responses of *mpv17*$^{-/-}$ control eyecups (gray bars). Four were found in *gnat2:trβ2* transgenics (magenta bars). Cone saturation amplitudes (Vm_i, Eq. 1, Fig.2A) are fractions of dataset maximum amplitudes (± SE). Asterisks (or n.s., not significant) represent the significance of differences (GraphPad Prism convention). Vu358 (UV, one sample test): $t(1579) = 4.81$, $p = 1.7 \times 10^{-6}$; Vb415 (B1): $t(2983) = 2.97$, $p = 0.0030$; Vg460 (G1): $t(2983) = 2.26$, $p = 0.024$; Vg480 (G3, one sample test): $t(1579) = 6.59$, $p = 6.1 \times 10^{-11}$; Vr556 (R2): $t(2983) = 1.52$, $p = 0.127$; Vr575 (R1): $t(2983) = 4.87$, $p = 1.2 \times 10^{-6}$. ***D***, Adult spectral curves for *mpv17*$^{-/-}$ and *gnat2:trβ2* cone signals. The transgene shifts sensitivity peaks to long wavelengths for all constant-quantal irradiances [3.4, 4.0, and 4.6 log(quanta·μm^{-2}·s^{-1})]. ***A***, ***B***, The log(k_{R1R2}) values are R1 or R2 cone semi-saturation irradiances in log(quanta·μm^{-2}·s^{-1}). ***A***, ***B***, ***C***, ***D***, 8-18-month adults, 10 mM Aspartate medium.

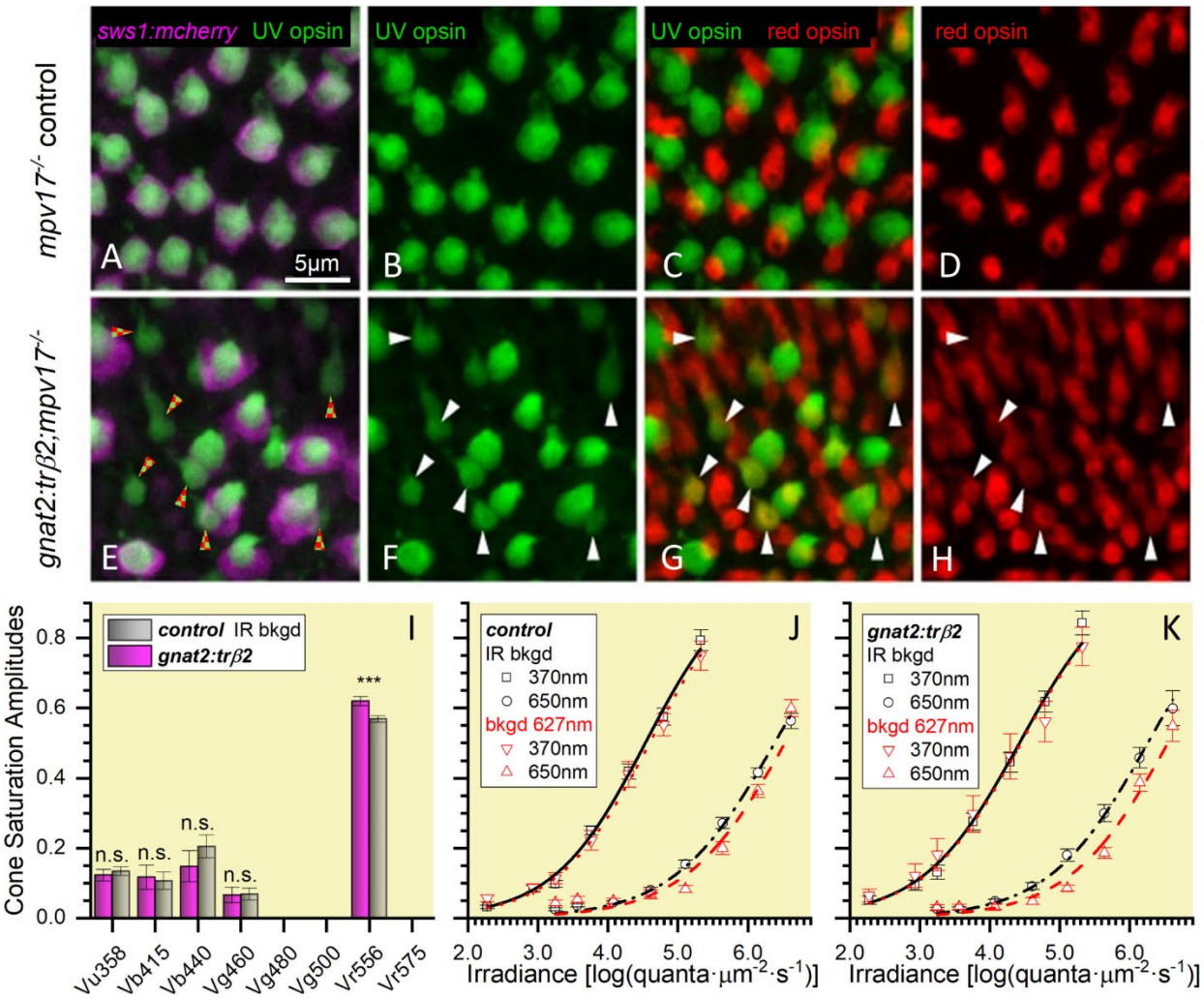

Figure 11. UV-red mixed opsin cones silence UV-opsin reporter expression but lack red-opsin light sensitivity. ***A***, UV-opsin (SWS1) immunoreactivity (green) and florescence of a reporter transgene for *sws1* (*sws1:nfsBmCherry*, magenta) colocalize in *mpv17*$^{-/-}$ control UV cones. ***B***, UV-opsin immunoreactivity in control retinas. ***C***, In the control retina UV-opsin (green) and red-opsin immunoreactivity (red) localize in separate cones. ***D***, Red-opsin immunoreactivity in the control retina. ***E***, In *gnat2:trβ2* cones, UV-opsin immunoreactivity (green) is always found when there is *sws1* reporter gene fluorescence (*sws1:nfsBmCherry*, magenta), but not all UV-opsin immunoreactive cones show reporter-gene fluorescence (red and green checkered arrowheads). ***F***, UV-opsin immunoreactive cones in the *gnat2:trβ2* retina. ***G***, Colocalization of UV-opsin (green) and red-opsin (red) immunoreactivity in *gnat2:trβ2* cones. White arrowheads (***F***, ***G***, ***H***) point to cones expressing both UV (green) and red opsins (red). The mixed opsin cones are the UV-opsin immunoreactive cones in ***E***, that lack *sws1* reporter fluorescence (red and green checkered arrowheads). ***H***, Red opsin immunoreactive cones in *gnat2:trβ2* retina. ***I***, Saturation amplitudes (V_{mi} in Eq. 1, Fig. 2A) of signals from cone types in control (grey) and *gnat2:trβ2* (magenta) eyes. Control: Spectral algorithm fit to 1890 datapoints from 27 datasets recorded in 15 eyes; *gnat2:trβ2*, 1260 datapoints from 18 datasets recorded in 11 eyes. In each case the optimal fit was model #79. The *t*-test and *p*-values are given in the text. ***J***, Control strain (*mpv17*$^{-/-}$) irradiance-response curves at 370 and 650 nm in the presence of infrared (IR) or 627-nm (red) backgrounds (bkgd). Control points are means ± SE (370 nm stimulus, IR background, *n* = 27; 370 nm stimulus, red background, *n* = 15; 650 nm stimulus, IR background, *n* = 54 or 27; 650 nm stimulus, red background, *n* = 30 or 15). ***K***, Gain-of-function *gnat2:trβ2* irradiance-response curves at 370 and 650 nm in the presence of IR or red backgrounds. Points are means ± SE (370 nm stimulus, IR background, *n* = 18; 370 nm stimulus, red background, *n* = 12; 650 nm stimulus, IR background, *n* = 18 or 36; 650 nm stimulus, red background, n = 12 or 24). ***J***, ***K***, Hill function curves fit at each background and wavelength are constrained to have equal maximal amplitudes and coefficients. Cone-PIII ERG signals isolated with 20 mM Aspartate. ***A***-***K***, Eyes and retinas are from 5-dpf larvae.

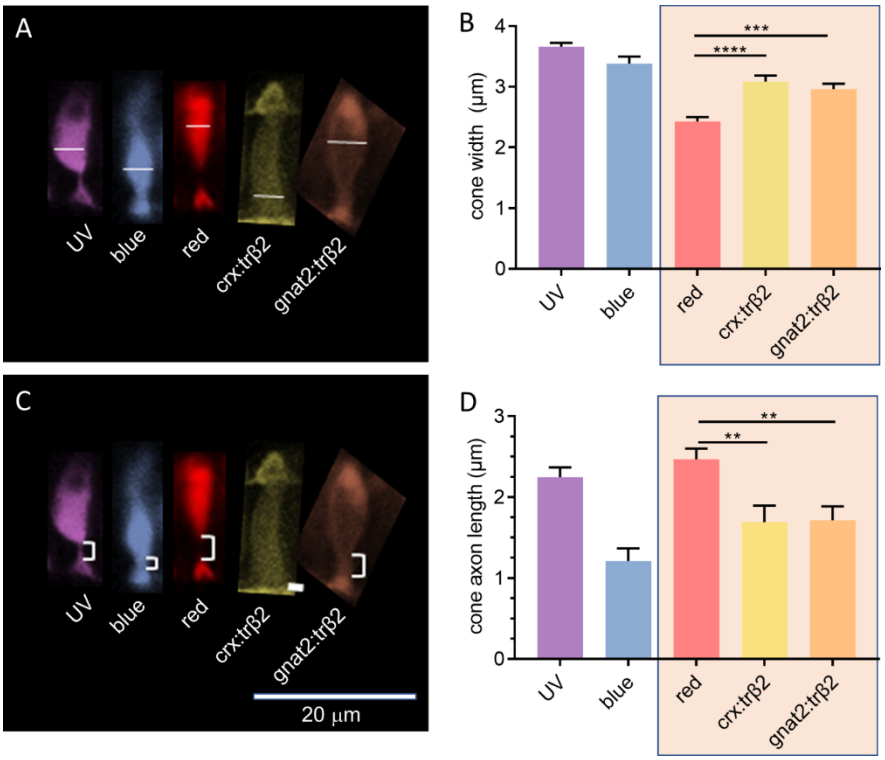

Figure 12. Thyroxin-receptor-β2 gain-of-function transgenes alter cone morphology. ***A***, Width of cone types identified by transgene markers, is measured at the greatest extent of the inner segment. ***B***, The trβ2 gain-of function cones are significantly wider than red-cones. ***C***, The cone axon length is measured from the base of the inner segment to the apex of the cone pedicle. ***D***, The trβ2 gain-of-function axon lengths are significantly shorter than red-cone axon lengths. ***C***, ***D***, Asterisks indicate significant differences (Graphpad convention, ANOVA and tukey-post-hoc *p*-values given in text). ***A***, ***C***, Images are of 6-dpf *in-vivo* larval fluorescent cones from confocal stacks. Control UV and red cones were imaged in *sws1:GFP;trβ2:tdTomato* larvae; blue cones, in *sws2:GFP* larvae; fluorescent trβ2 gain-of-function cones, in *crx:mYFP-2A-trβ2* and *gnat2:mYFP-2A-trβ2;mpv17*$^{-/-}$ larvae. Larvae were anesthetized with MS222 and embedded in agarose after raising to 6 dpf in 300 μM PTU to block melanin formation in the pigment epithelium.

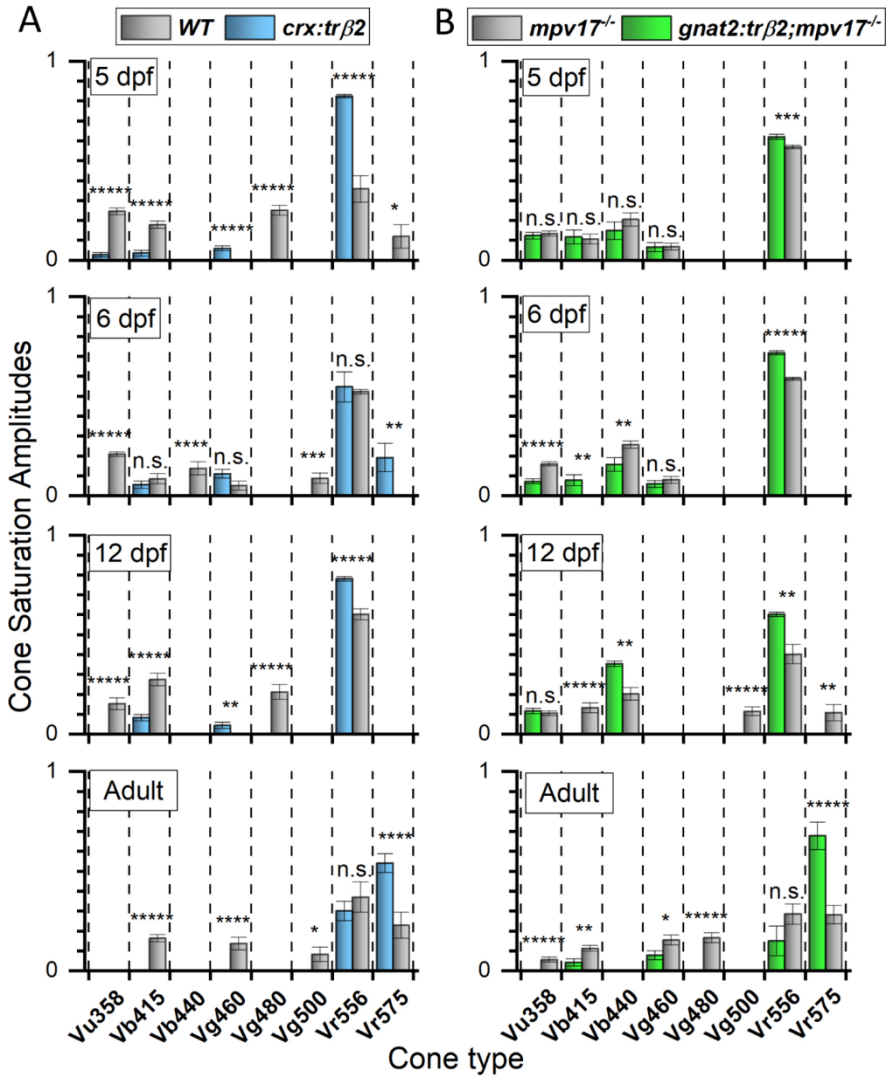

Figure 13. Signal development in red-, green-, blue- and UV- cone types. ***A***, Throughout development red-cone signals (Vr575, Vr556) are larger than WT in *crx:mYFP-2A-trβ2* while blue-, green- and UV- cone signals (Vb415, Vb440; Vg460, Vg480, Vg500; Vu360) are smaller, disappearing with time. ***B***, Signal amplitudes of red, green and blue cones in *gnat2:mYFP-2A-trβ2;mpv17*$^{-/-}$ are indistinguishable from *mpv17*$^{-/-}$ (*roy orbison*) controls at 5 dpf but red-cone amplitudes increase while green-, blue- and UV- cone signals decrease later in development. ***A***, ***B***, '5 dpf' and '6 dpf' are larval or embryonic stages. '12 dpf' is a juvenile stage and 'Adult' is 8-18 months. In each bar chart spectral datasets from multiple eyes are combined to yield *n* total response amplitudes and fit by the equation 1 (Fig. 1) algorithm to model the contributing cone types and their saturation voltages. ***A***, 5 dpf: WT, 7 eyes, *n* = 847; *crx:trβ2*, 11 eyes, *n* = 1669. 6 dpf: WT, 10 eyes, *n* = 1858; *crx:trβ2*, 11 eyes, *n* = 1860. 12 dpf: WT, 3 eyes, *n* = 253; *crx:trβ2*, 6 eyes, *n* = 1341. Adult: WT, 14 eyes, *n* = 1400; *crx:trβ2*: 16 eyes, *n* = 1470. ***B***, 5 dpf: *mpv17*$^{-/-}$, 15 eyes, *n* = 1890; *gnat2:trβ2*, 11 eyes, *n* = 1260. 6 dpf: *mpv17*$^{-/-}$, 15 eyes, *n* = 1945; *gnat2:trβ2*, 17 eyes, *n* = 1540. 12 dpf: *mpv17*$^{-/-}$, 16 eyes, *n* = 1820; *gnat2:trβ2*$^{-}$, *mpv17*$^{-/-}$, 9 eyes, *n* = 770. Adult: *mpv17*$^{-/-}$, 13 eyes, *n* = 1610; *gnat2:trβ2*, 11 eyes, *n* = 1400. For *t*-tests, a cone only detected in one of the two strains is evaluated by a one-sample *t*-tests, so that asterisks denoting significance (Graphpad convention, n.s., not significant) either compare detected transgenic and control amplitudes for a cone type or show the significance > 0 for a single detected amplitude. Additional *F*-test, *t*-test and *p* values are in the text.